9-15-2016

Orbit Determination Using Vinti's Solution

Steven P. Wright

ORBIT DETERMINATION USING VINTI'S SOLUTION

DISSERTATION

Steven P. Wright, Major, USAF

AFIT-ENY-DS-16-S-067

DEPARTMENT OF THE AIR FORCE
AIR UNIVERSITY

AIR FORCE INSTITUTE OF TECHNOLOGY

Wright-Patterson Air Force Base, Ohio

The views expressed in this dissertation are those of the author and do not reflect the official policy or position of the United States Air Force, the Department of Defense, or the United States Government.

AFIT-ENY-DS-16-S-067

ORBIT DETERMINATION USING VINTI'S SOLUTION

DISSERTATION

Presented to the Faculty

Graduate School of Engineering and Management

Air Force Institute of Technology

Air University

Air Education and Training Command

in Partial Fulfillment of the Requirements for the

Degree of Doctor of Philosophy in Astronautical Engineering

Steven P. Wright, B.S., M.S.

Major, USAF

September 2016

AFIT-ENY-DS-16-S-067

ORBIT DETERMINATION USING VINTI'S SOLUTION

Steven P. Wright, B.S., M.S.
Major, USAF

Committee Membership:

Dr. William E. Wiesel
Chair

Dr. Ronald J. Simmons
Member

Dr. William P. Baker
Member

Lt Col Scott G. Putnam, Ph.D.
Member

ADEDEJI B. BADIRU, Ph.D.
Dean, Graduate School of Engineering
and Management

Abstract

Orbital altitudes congested with spacecraft and debris combined with recent collisions have all but negated the Big Sky Theory. As the sheer number of orbital objects to track grows unbounded so does interest in prediction methods that are rapid and minimally computational. Claimed as the "other solvable solution," the recently completed solution to orbital motion about the earth, based on Vinti's method and including the major effects of the equatorial bulge, opens up the prospect of much more accurate analytical models for space situational awareness. A preliminary examination of this solution is presented. A numerical state transition matrix is found using Lagrange partial derivatives to implement a nonlinear least squares fitting routine. Orbit fits using only the solvable solution for non-circular, non-equatorial trajectories less than 60 degrees inclination are on the order of a few hundred meters with projected, average error growth of less than a kilometer per day which is similar to the expected performance of the Air Force's method. Also, a classical perturbations approach to incorporate the dissipative effects of air drag using Hamiltonian action and angle formulation is developed. Predicted drag effects are 97.5% correct after one day and 87% correct after five days when compared to an integrated truth. Results are validated by performing a similar method on the two body problem.

For my children, the smallest yet greatest sources of my motivation

Acknowledgments

Many thanks to Dr. Wiesel for guidance and advice throughout this incredible learning experience.

The most valuable...yet toughest...lesson I learned at AFIT was the more I learned, the more I realized I did not know. I believe this humbling experience is the true test of a doctoral student. I can certainly now appreciate that education is not a destination but a journey.

I am incredibly blessed to have grown up in a loving environment that taught me how to work hard (but play harder), love truly, and believe in myself. I was always encouraged to follow my dreams through stubborn determination driven by unbounded imagination. I thank my family and all those I call family for helping lay the foundation necessary to get what I want out of life while being a good steward with what God has given me.

This accomplishment could not remotely be possible if not for my amazing wife. Her patience, encouragement, and support are limitless. For tolerating all the missed family time, absent Saturdays, and distracted conversations, I am tremendously grateful. You are truly one in a million.

Above all, thanks to God for salvation, strength to face adversity, and a creation that becomes more fascinating the more we learn about it.

Steven P. Wright

Table of Contents

Page

Page

List of Figures

List of Tables

List of Symbols

Symbol	Definition
J_k	k-th zonal geopotential coefficient
L, G, H	Delauney momenta
l, g, h	Delauney coordinates
M	mean anomaly
ω	argument of perigee
Ω	line of nodes
i	inclination
e	eccentricity
$\mathbf{X}$	state vector
$\delta\mathbf{X}$	some incremental change in the state vector
t	time
t_0	initial or epoch time
Φ	state transition matrix
$\mathbf{z}$	observation or measurement vector
$\mathbf{G}$	observation relationship function
H	linearized observation relationship function
T	linearization of observation multiplied by state transition matrix
Q	weighting matrix to input process noise
$\boldsymbol{r}$	residual vector
$\mathbf{r}, \mathbf{v}$	position, velocity vector
σ	standard deviation
α_k, β_k	Vinti separation momenta and coordinates
DU	geocentric distance unit

Symbol	Definition
TU	geocentric time unit
ρ	air density
B^*	drag parameter
C_D	drag coefficient
m	satellite mass
A	satellite frontal area
$\mathcal{I}_k, \theta_k$	action-angle variables
ω_k	basis frequencies corresponding to angle coordinates
$\mathcal{FS}$	periodic portion of Fourier series vector
$\mathbf{j}$	vector summation index
$\boldsymbol{C}_\mathbf{j}, \boldsymbol{S}_\mathbf{j}$	vector cosine and sine coefficients
ρ, c, η, ϕ	Vinti's oblate-spheroidal coordinates

List of Acronyms

Acronym	Definition
AFIT	Air Force Institute of Technology
AFSPC	Air Force Space Command
ASAT	Anti-Satellite
DARPA	Defense Advanced Research Projects Agency
ESA	European Space Agency
GPS	Global Positioning System
JSPOC	Joint Space Operations Center
KAM	Komolgorov, Arnold, Moser
LEO	Low Earth Orbit
MMOD	Micro-Meteroid and Orbital Debris
NSSCC	National Space Surveillance Control Center
OD	Orbit Determination
PPT	Positions and Partials with Respect to Time
RMS	Root Mean Square
RSS	Root Sum Square
SGP	Simplified General Perturbations
SOCRATES	Satellite Orbital Conjunction Reports Assessing Threatening Encounters in Space
SP	Special Perturbations
SSN	Space Surveillance Network
STK	Systems Tool Kit
TBP	Two Body Problem
TLE	Two-line Element Set

Acronym	Definition
UKF	Unscented Kalman Filter
WPAFB	Wright-Patterson Air Force Base

ORBIT DETERMINATION USING VINTI'S SOLUTION

I. Introduction

1.1 Motivation

On 12 February 2009, an active US communications satellite, Iridium-33, and an inactive Russian satellite, Cosmos-2251, collided at an altitude of approximately 790 km. This marked the first known accidental collision between spacecraft payloads. The resulting debris was estimated to range between 1,000 and 2,000 objects greater than 10 cm and between 60,000 and 120,000 objects greater than 1 cm [1]. Later that same year, the USSTRATCOM Commander at the time, General Kevin Chilton, claimed that the Big Space Theory came to a close with this seminal event. In other words, no longer can the space community claim the probability of collision with other orbiting objects, due to the sheer size of space, is low enough to be ignored [2].

Due to orbital changes experienced by the scattering of particles upon impact, this significant debris cloud has been dispersed near globally and now congests this highly populated altitude regime.[1] According to the US Air Force, as of 1 March 2013, it continued to track 2,160 pieces from this collision alone [3]. This number is approximately 1,530 as of 26 May 2015 [4].

In the days prior to the collision, a close approach of these two spacecraft was predicted by SOCRATES.[2] An avoidance maneuver was not performed prior to the collision,[3] and, with perfect hindsight, it could be surmised this was completely

[1] In the week prior to the incident, it was reported that approximately 1,050 objects would come within 5 km of any one of 66 satellites in the Iridium constellation

[2] SOCRATES is a public service to the international satellite community provided by the Center for Space Standards & Innovation (CSSI) - www.celestrak.com/SOCRATES

[3] Only Iridium-33 had the capability for maneuver

preventable. However, this was not the only near miss for that week and not even the most probable or closest predicted. The miss distance predicted for that conjunction ranged between 117 m and 1.812 km across reports, while the closest projected approach between several other crafts averaged between 30 and 50 m [5].

It would seem plausible to assume that if a craft made it on the list of probable conjunctions, an avoidance maneuver should be planned and executed. However, significant mission trade-offs can occur with even the smallest burn. Some missions require coming off-line for a period of time causing unneeded outages. Inevitably, propellant mass is lost that is ultimately intended to maintain the payloads' life expectancy. Therefore, a serious cost-benefit analysis is required for each possibility of a close call. Planning for a maneuver can be time-intensive as well, requiring several hours or even days. What makes this decision practical is an accurate estimate of both crafts' position and velocity at the future time in question, therefore giving a realistic probability of collision.

Unfortunately, using the data available to determine that this conjunction was significant in the midst of the dozens of others at the time, is "simply not possible" according to Kelso [6]. It is surmised the amount of covariance or uncertainty in the position estimate becomes greater than the miss distance in these notices. Statistical significance of this information is lost due to the lack of actionable information.

An increase in accuracy of current satellite state estimates combined with a lack of error growth over time would revolutionize conjunction analysis. The vast number of false positive warnings would drastically drop and statistics would become reasonable. According to General Robert Kehler, the Commander of Air Force Space Command at the time of the collision, 10,000 conjunction warning messages were generated by the Joint Space Operations Center (JSPOC) in 2012 but only 75 maneuvers were performed in response [7]. Conservatively, assume those 75 instances would actually have resulted in a collision if no action were taken. This means the warnings issued indicate less than

a 0.75% chance of an unplanned rendezvous. Realistically, this statistic is probably much lower but the calculated probability does not accompany the warning [8]. If accuracy is improved, these messages to vehicle operators could become meaningful with enough lead time to formulate an efficient course of action.

For example, consider a small maneuver of 1 cm/sec. If this was performed one hour before conjunction, it would result in a position change of 36 m, which is potentially still in harm's way. However, if the same maneuver is accomplished the day prior, the craft would be 8.6 km away from danger at that time.

1.1.1 Department of Defense Concerns

1.1.1.1 Legacy Analytical Propagators

The US Department of Defense (DoD) maintains two sets of mathematical models to calculate and predict position/velocity vectors of objects in low earth orbit (LEO), Simplified General Perturbations-4 (SGP4) and Positions and Partials with Respect to Time-3 (PPT3). They both utilize analytical theory and are originally derived and modified from Kozai and Brouwer's solution (see Chapter II). Using these programs to update state vectors for all foreseeable objects in orbit constitutes maintaining an extensive catalog of satellites and orbital debris for space situational awareness purposes.

With the exception of updates to account for more objects or modernize interface issues and computer processes within, there have been no updates to the underlying theory in over 50 years [9]. Specifically, Vetter claims the last "evolutionary growth" of theory pertinent to SGP4 and PPT3 occurred in 1962 and 1964, respectively. To put this in military perspective, air superiority workhorses of that time included the F-102 Delta Dagger and the B-47 Stratojet. Since then, significant updates to orbital solution theory have been specific to special perturbation techniques to coincide with and exploit the dawn of the computer age [10].

1.1.1.2 Accuracy of SGP4

Although the actual accuracy of SGP4 is unknown and can change significantly based on several factors including orbital altitude and shape, it is generally known to be not very accurate. Its benefit and utility have long been advertised as a first cut solution to give to integrators. Levit labels predictions generated from SGP4 as "not sufficiently accurate to warrant maneuvering to avoid collision" by mentioning it creates too many possibilities of collisions with each having a low probability [11]. This could be likened to the statement concerning the conjunction assessment lacking statistical meaning (see §1.1).

Levit goes on to quantify the error growth of a new method as 100 m per day and says this would be a "10 fold" improvement upon SGP4. One can infer, on average, that SGP4 can be expected to have one kilometer of error growth per day. Greene introduces a method to integrate GPS readings into SGP4 propagation estimates and quantifies unreasonable growth rates as 1 km per day [12]. Dong and others evaluate an unclassified version of SGP4 at different orbital altitudes with different parameters. Solution errors for near-earth objects are reported to be on the order of a few hundred meters with the vast majority being under 10 km. The error growth over the sampled orbits is determined to be less than 40 km over 3 days for LEO satellites and only 1 day for those with elliptical orbits [13]. Vetter agrees by saying the analytical theory of this, and similarly PPT3, are only accurate to a 1-10 km level [10].

To be clear, SGP4 does not calculate miss distance for specific conjunctions. Rather, it provides a screening of all active satellites for possible close approaches. If certain criteria are met, then relevant information is handed over to more accurate systems for further analysis. However, these other algorithms utilize numerical integration and take much longer. So, if the first cut was more accurate, time spent analyzing meaningful conjunctions would be minimized by avoiding those that have zero chance. System time could be opened up for other, more relevant tasks.

1.1.1.3 Orbital Debris

The world's leading orbital tracking entity, the US Space Surveillance Network (SSN), tracks over 23,000 objects in LEO larger than 10 cm, or about the size of a softball. It is estimated there are upwards of 500,000 objects smaller than this that are not being tracked. Of all the objects tracked, only about 5% of these, or about 1,300, are active satellites [14]. The rest are considered debris, or junk. Currently, to maintain the catalog of over 23,000 objects, the SSN produces over 200,000 sensor taskings, which return around 320,000 observations to be processed every day. The expected activation of the Space Fence at the Kwajalein Atoll will provide the ability to track objects as small as 2 cm. It is clear that the amount of data available to the tracking network will instantaneously multiply astronomically.

In late 2014, the Orion crew capsule orbited the earth twice and then experienced re-entry as part of an experimental test flight (Orion EFT-1). With a flight duration of almost 4.5 hours, the orbital altitude ranged from 200 km to 5,808 km. Post-flight analysis examined the recovered portion[4] of the craft's body for damage and found 25 regions of interest. After further investigation, six of these were determined to be potentially due to collisions with micro-meteroid and orbital debris (MMOD) [15]. Although the size of these impact craters were on the order of millimeters, this gives reason for alarm. A flight with such short duration managed to collide with several objects that are too small to track.

1.1.1.4 Debris Growth

Behind risks from launch and deployment, the European Space Agency (ESA) claims space debris collision ranks as the third highest danger to many missions [16]. In 2008, Liou and Johnson advertised some near-earth orbital regimes had reached a critical density where future collisions between any combination of active satellite, rocket body, or debris would be inevitable [17]. This would lead to a creation of more objects kicking off a chain

[4]The forward bay cover was jettisoned during parachute deployment and sank before recovery

reaction and ultimately create an unusable orbital region consisting of a debris cloud. This was termed the Kessler effect in 1975 [18].

It could be argued that the realization of Liou's projection occurred with the Iridium-33/COSMOS-2251 collision. To provide further evidence, on 22 January 2013 a tiny Russian satellite named BLITS[5] collided with a piece of debris from the infamous Chinese ASAT test of 2007 [19]. These are not the only collisions to have occurred in recent years, only the most public.

1.1.1.5 Risk Avoidance

There is no shortage of ideas for avoiding the risk inherent with orbital debris growth. At present, methods for actual debris removal from orbit are just that, ideas. The Defense Advanced Research Projects Agency (DARPA) has initiated the Catcher's Mitt study to investigate lowering the number of useless objects in orbit. Objectives include modeling the orbital debris problem coupled with its expected growth and exploring technical methods of debris remediation. [20]

In support of this study, DARPA commissioned the RAND National Defense Research Institute to pose the problem in a global, strategic light. The resulting report, *Confronting Space Debris*, compares the current problem to other globally impacting risks such as acid rain, airline security, and oil spills to name a few. Characteristics of each issue are identified within categories such as stakeholders, blameworthy/affected parties, and mitigation/remediation strategies.

1.1.2 Recent Findings

The National Research Council of the National Academies published a study named *Continuing Kepler's Quest: Assessing Air Force Space Command's Astrodynamics Standards* in 2012 at the request of Air Force Space Command (AFSPC). It examined and reviewed current standards in which the AF uses algorithms and computer systems

[5]Measuring only 6.7 inches in diameter and weighing a mere 16.2 lbs, BLITS is classified as a nanosatellite

to maintain awareness of thousands of orbiting objects. Among several suggestions and findings were those including analytical methods and the command's understanding of modern dynamical systems. [8]

Although special perturbations has widespread popularity for modern innovation and accuracy in specialized applications, the council wanted to re-emphasize the importance of updating and modernizing general perturbations methods. This will allow continued interfacing ability with international satellite users while decreasing the computational load demanded from numerical integrators by delivering a more accurate initial solution.

On the subject of the organization's knowledge of modern dynamical theory, the studies' comments were scathing. Not only did the committee find a "striking omission" in modern theory employed, they were not convinced the experts were even aware of such advancements. It was reported that much insight into the behavior of dynamical systems, which is critical to carrying out AFSPC's mission, can be gained by no longer depending solely upon theory untouched since the 1960s.

1.2 Approach

Over 50 years ago, Dr. John Pascal Vinti created an elegant orbital solution using analytical techniques considered advanced even by today's standards [21]. Due to the sophisticated nature of his techniques and a lack of self promotion, this field and the DoD has all but forgotten his effort [22:1]. Wiesel demonstrates that Vinti's solution can be put through modern numerical techniques to make it very relevant today with the potential to rival current methods [23]. This is the starting point for the current work.

First and foremost, Wiesel's method requires a state transition matrix. Not only is it required by least squares fitting, it is needed to perform meaningful analysis and development. Although analytically finding this matrix is preferred, the author proceeds with a version developed using numerical differentiation techniques.

Once local orbital motion described through Vinti's solution is available with the state transition matrix, it can be analyzed for accuracy and viability. A least squares orbit fitting routine is developed and employed with simulated data generated using a numerical integration truth model. Various comparisons are first made using Vinti's model for the earth's geopotential (to be discussed in §2.5). Observations affected by the full geopotential (to order and degree 20) are then generated and fit to examine initial performance that should resemble reality. For perspective, this performance is compared to that of an unclassified version of SGP4 .

As a demonstration of the capability inherent in Vinti's solution, an example of adding a major perturbation is presented. Accounting for air drag is demonstrated using the action-angle formulation and classical perturbation theory; this nonlinear effect is sampled and then transformed into multiple Fourier series that can be analytically integrated. Having this expression provides a function of time for rapid calculation within orbit fitting. For validation, the same technique is performed with action-angle variables found using the two body problem (TBP) method.

1.3 Problem Statement

The recently completed solution to orbital motion about the earth, based on Vinti's method and including the major effects of the equatorial bulge, opens up the prospect of much more accurate analytical models for space situational awareness. In particular, prediction of conjunctions absolutely requires accuracies of a few meters, at worst, to eliminate the excessive false positive rate of Space Command conjunction messages. The new solution will be evaluated against simulated satellite data to assess its accuracy. With potential upgrades to the theory, this required accuracy for collision avoidance could be attained. In addition, the solution's utility for incorporating additional perturbations such as air drag is examined.

1.4 Results

When the newly revised orbital solution is used as the analytical propagator for an orbit fitting routine, results are promising. For orbits only perturbed by the full geopotential, errors are generally on the order of hundreds of meters. When compared to an unclassified version of SGP4, results were only worse than this for a few orbital regimes. Otherwise, Vinti was superior or, at the least, very similar. Although this method does not currently outperform numerical integration, it could rival it after further perturbations are accounted for in future works.

The problematic exceptions to the performance described above are when inclination increases past 65^o. Errors rise to over 10 km for low eccentricity and more than 60 km for high eccentricity. When inclination increases past 82.5^o a solution is no longer calculable due to a numerical flaw in the integrals deep in the revised solution. Valid results return when inclination reaches 97.5^o and mirrors the behavior below polar. The author believes this difficulty is due to the negative argument of perigee rotation rate that occurs between the two critical inclinations of 63.4^o and 116.6^o. Fixing this flaw is not within the scope of the current research.

Also, a solution is not available for eccentricity and inclination of exactly zero due to the root finding method unique to the new theory which requires a definite perigee and northernmost point. However, errors did not grow as these values approached zero. Eccentricity and inclination as low as 0.001 and 0.01^o, respectively, returned satisfactory results.

When air drag is accounted for through a novel general perturbations approach, the utility of Wiesel's solution is demonstrated. Angle perturbations are calculated and found to be 97.5% accurate after one day and 87% after five days. These numbers are validated through a parallel effort using TBP variables.

1.5 Overview

The document is organized into seven chapters. This first chapter has provided insight and motivation behind what makes this research relevant. Chapter II discusses historical context behind the development of analytical orbital solutions as it pertains to space situational awareness and catalog maintenance. Vinti's solution and modifications made by Wiesel are also presented. Chapter III introduces a method for applying the new Vinti solution to an orbit fitting routine. A numerical state transition matrix is developed and initial fitting results are examined. Chapter IV summarizes results from performing orbit fitting on an orbit in a full geopotential using the Vinti solution as modified by Wiesel which uses an approximated potential. Chapter V presents a novel approach for incorporating air drag perturbations using action-angle variables. This approach demonstrates the utility in applying Wiesel's solution in a general perturbations context. Chapter VI uses the approach presented in Chapter V but with TBP variables as a comparison. Chapter VII provides conclusions and future work recommendations. An appendix with extra graphs exploring a wider range of orbital parameters is included. The author assumes a prior knowledge of Hamiltonian mechanics as it applies to orbital dynamics and at least an entry level understanding of estimation theory. All computer code is developed in C++ with double precision accuracy wherever possible in units of nondimensional, earth-centered distance and time units.

II. Background

This chapter lays the groundwork necessary to appreciate using the Vinti method as a modern analytical solution for earth-orbiting objects, be it spacecraft or debris. A brief history of orbit determination, as it applies to space surveillance and tracking, is provided. Also, a few classical solution methods critical to that history are discussed.

2.1 Watching the Skies

With the launch of Sputnik in 1957, the military mission of space surveillance was born. Although the small innocuous object only transmitted beeps continuously, it implied that an adversary on the other side of the globe maintained the technological capability to reach American soil. Therefore, an awareness of orbital objects' flight paths was desired.

The country needed a way to not only determine the location of an enemy spacecraft but predict where it would be in the foreseeable future. This awareness was desired by the Navy to warn battle fleets against possible reconnaissance. Also, if a satellite could pass overhead, capabilities definitely existed to deliver a weapon across the globe. So, as the Air Force needed to provide early warning for such incoming threats, object differentiation was critical. It was paramount that they had the capability to unequivocally determine between a known satellite trajectory and an inbound warhead.

To this end, a formal effort to catalog all known orbiting objects was initiated in 1959 by the National Space Surveillance Control Center (NSSCC) at Hanscom Field in Bedford, MA. Receiving observations by way of teletype, telephone, mail, and personal messenger, orbital predictions were produced using relatively primitive methods, then distributed. These predictions included estimated times of passage through the ascending node with corresponding longitude for the next few days. Observation sites also received information regarding where to look in the sky when objects flew by [24].

Over the next decade, the number of objects in orbit rose as did the tide of international tensions. Therefore, the community desired increased accuracy of orbital predictions through more sophisticated methods. Numerical solutions resulting from special perturbations (to be discussed in §2.3.2) provided higher accuracy but at the cost of saturating computer systems of that era.

2.2 Evolution of Analytical Theory - A Snapshot

Project SPACETRACK was commissioned to seek new and relevant analytical solutions describing orbital motion to support catalog maintenance. In the same edition of Astronomical Journal in November of 1959, Dirk Brouwer and Yoshide Kozai published two different orbital solutions [25; 26]. Most analytical models in use today still have one of these two original formulations as their foundation [24].

Published in 1959, Brouwer's solution to orbital motion has been widely used and regarded as a benchmark of artificial satellite theory. He performs canonical transformations to simplify the equations of motion using the canonical Delauney variables. In terms of the classical orbital elements, these are

$$\begin{aligned} L &= \sqrt{\mu a} & l &= M \\ G &= L\sqrt{1-e^2} & g &= \omega \\ H &= G\cos i & h &= \Omega \end{aligned} \tag{2.1}$$

He accomplishes this change of variables using a geopotential derived from a spherical reference frame, shown in Figure 2.1. Spherical coordinates are related to the cartesian frame through

$$\begin{aligned} x &= r\cos\theta\sin\phi \\ y &= r\sin\theta\sin\phi \\ z &= r\cos\phi \end{aligned} \tag{2.2}$$

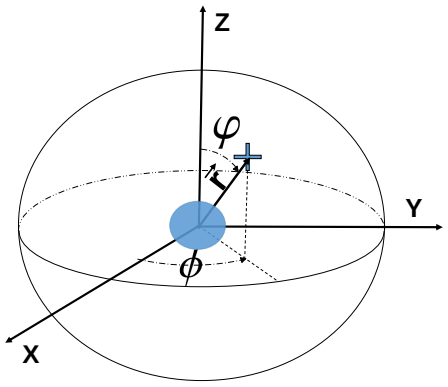

Figure 2.1: Spherical Reference Frame

He then expands the disturbing function using von Ziepel's method. This provides short and long period terms to order J_2 and secular motion to order J_2^2. The Hamiltonian for this model already lacks the right ascension of the ascending node, Ω, but his transformations also causes argument of perigee, ω, and the mean anomaly, M, to drop out. This causes the conjugate momenta, L, G, H to be constant. Through truncated expansions, this method accounts for the earth's asphericity, J_2 through J_5, and is expressed in terms of a set of mean elements [27:688].

Kozai generated a first order solution that has rivaled mainstay orbital solutions to this day. He uses an ad-hoc averaging technique of Lagrange's Variation of Parameters, which is inherently fast as a computing method [27:688]. In 1962, he went on to derive an extension of Brouwer's original solution [28].

Also in 1959, Garfinkel attempted a similar method to Brouwer [29]. Using von Ziepel's method with Delauney variables, the most noticeable departure in theory is the

form of the geopotential used. However, Garfinkel claimed his results were similar to those of Brouwer.

Over the next decade, development of analytical orbital theory continued mostly in the context of modifying and adding to the original solutions of Brouwer and Kozai. It was in these solutions that the US Air Force's analytical orbital solution software, SGP, was rooted with its genesis in the early 1960s [24].

Lyddane significantly improved Brouwer's solution by implementing Poincaré variables with which to solve the system [30]. Before, singularities existed at low inclination and eccentricity and at the critical inclination. This change of variables preserved the benefits of the solution while avoiding problematic results. Similar to Poincaré's approach, Deprit addressed problems at the critical inclination [31].

Lyddane's modification of Brouwer's solution became the defining characteristic that set apart the US Navy's analytical propagator, PPT, or Positions and Partials with respect to Time. The US Air Force's SGP continued with a modified blend of Kozai and Brouwer's theory until later adopting Lyddane's modification in SGP4 [24]. Brouwer and Hori attempted to incorporate drag effects by using a static exponential representation for atmospheric density with a constant scale height [32]. This complex model was so extensive for computers at the time that it was operationally infeasible. Simplified treatment of the density profile allowed improvements first by Lane, then by Lane and Cranford [33; 34]. These improvements as well as Lyddane and Deprit's modification were key to the development and implementation of SGP4.

Significant improvement in orbital theory and operations occurred in this turbulent decade of the 1960s. However, in these early years of space tracking, solutions were accurate enough if they simply provided acceptable look angles and flyover times. Conjunctions or close flybys of other spacecraft or objects were almost inconceivable due to

the Big Space Theory, a derivative of the Big Sky Theory. Concerning these improvements specific to Brouwer's theory, Vallado says:

> All these developments give Brouwer's method the appearance of being a superb analytical theory, but it has several significant shortcomings. It's fine for general use in applications needing limited accuracy. But as computational power increases and satellite systems demand more accuracy, its effectiveness diminishes - it's still an analytical series approximation accounting for a large but incomplete subset of dominant perturbations, so it's only moderately accurate. The U.S. Air Force and Navy operate similar versions of this theory. [27:690]

So, in this modern context, the community should not remain complacent with the confidence in a traditional method merely because it has been used for decades.

In the past, if more accuracy was needed for a certain orbit, analytical theory was put aside after a first cut solution was obtained. The numbers were then handed over to numerical integrators. This is still true today, however, in the past the solution was more accurate at the expense of computing time for the rest of the afternoon. Although computing time necessary for this alternate approach has reduced significantly, rapid analytical solutions still have value. This is especially true for those that are actually accurate enough to be meaningful. Using these two different methods for orbital prediction will be discussed in the next section.

2.3 Orbit Determination Methods

Determining the unique elements of a satellite's orbit is only as useful as how well those elements can be used to predict where that craft will be at a specific time in the future. The accuracy of such a forecast depends upon the model used in such a calculation. Predominantly, there are three types of orbit fitting/determination: general perturbations, special perturbations, and semianalytical techniques. The latter combines aspects of the first two and will not be reviewed in this work due to the wide variety of techniques used and lack of extensive documentation. Only the fundamental premises behind the first two approaches will be presented.

2.3.1 General Perturbations

Also known as analytical theory, Vallado explains that "General Perturbations techniques replace the original equations of motion with an analytical approximation that captures the essential character of the motion over some limited time interval and which also permits analytical integration" [27:609]. So, instead of describing the unique motion with exact solutions, successive approximations are made using various techniques. These expressions are generally valid for all initial conditions but only for a limited amount of time. Not unique to orbital mechanics, many disciplines utilize this methodology in obtaining useful physical descriptions of their systems of choice. The solutions of Kozai, Brouwer, and Garfinkel fall into this category.

However, expanding the expressions analytically can quickly get overly complex. More often than not, only second order solutions are provided due to these difficulties. Neglecting higher-order effects obviously degrades the accuracy but it makes a solution attainable. Also, describing the motion in such a way can provide valuable insight into the inner workings of the dynamics to aid in stability or ancillary studies. Although the derivations are arduous, computing time for a solution is minimal. This analytical method was commonplace before modern computing techniques opened the possibility of rapid numerical integration, bringing special perturbations to the forefront.

2.3.2 Special Perturbations

In the modern age of computing, special perturbations has been the leader of accurate OD schemes and orbital propagation. This involves capturing perturbations as accelerations in accurate equations of motion that can be numerically integrated using a wide range of methods and schemes. A specific orbit is defined by a set of initial conditions and then is integrated until a time of interest is reached. But, as the name would indicate, a particular solution is unique, or special, and cannot be used for analyzing other orbits; the process must be re-initiated for a new set of initial conditions. This is unlike general perturbations ,

where an analytical solution is valid for any set of initial conditions. Also, due to truncation and roundoff errors inherent in the integration, errors build up as the square root of the number of calculations made [35:2].

Coffey has introduced a way for the Navy to perform catalog maintenance using special perturbations [36]. He contends that accuracy will increase while mission requirements will be maintained. He uses a parallelized computing approach and says to "just add more [computer] processors" when the immense volume of tracked objects saturates the system. This statement about tracking all the objects with SP was made when the cataloged items was on the order of $20,000$. If the nation begins tracking objects as small as 2 cm after bringing a new Space Fence online, the catalog would suddenly grow to over half a million and instantly multiply processing time for any system attempting to track them all [14].

2.4 Space Surveillance and Tracking

Analytical propagators help maintain situational awareness over all objects in the catalog. They also provide various tools and information to the satellite community, including look angles[6] and initial conjunction analyses. When increased accuracy for a few objects is needed, the trajectories are analyzed further by integrators.

In keeping a database of thousands of objects, general perturbations wins out in keeping up with them all because only one computer call is necessary to provide state information for a given time in the future. Special perturbations would have to perform calculations at each time step from epoch until desired time. Although the estimate would probably be more accurate, even today's computers could potentially be overburdened performing such operations on thousands of satellites simultaneously.

The reduced complexity in computing combined with the ability to quickly approximate a state vector sometime in the future surely makes analytical theory attractive for

[6]This tells the user where to point the antenna for uplink/downlink purposes

space situational awareness as it applies to catalog maintenance. The current research examines a new solution that maintains computing benefits of general perturbations yet with potential to approach numerical integration accuracy.

2.5 Vinti's Solution

Return to that pivotal point in history when the US was racing to modify current methods to maintain situational awareness in the race for space. The preponderance of analytical solutions utilized spherical coordinates as discussed earlier. Using this reference frame, the Hamiltonian for two body motion can be separated and give a starting point from which to begin adding perturbations. However, this approach only results in one fundamental frequency from which to begin, termed fully degenerate.

Going almost unnoticed in the shadow of the likes of Brouwer and Kozai, John Pascal Vinti posed a unique departure in theory. Leveraging his physics background, he introduced an elegant oblate-spheroidal coordinate system to describe the orbital motion as perturbed by the earth's zonal effects [21]. Illustrated in Figure 2.2, the spheroidal coordinates are related to the physical ones through the expressions

$$\begin{aligned} x &= \sqrt{(\rho^2 + c^2)(1 - \eta^2)}\cos\phi \\ y &= \sqrt{(\rho^2 + c^2)(1 - \eta^2)}\sin\phi \\ z &= \rho\eta \end{aligned} \tag{2.3}$$

where ρ determines the size of the spheroid and is approximately the radius and c is a constant that determines the shape. For earth, c is set equal to J_2 times the radius of the earth squared. The right ascension of the satellite is ϕ and η determines the shape of the confocal hyperboloids of revolution.

Due to the orthogonality introduced between the reference frame and the effects due to zonal influence, developing the gravitational potential using this reference frame exactly accounts for J_2 and almost 75% of J_4. Then, performing a change of variables within this frame leads to separability of the perturbed Hamiltonian-Jacobi equation. Separating this

equation was Brouwer and Kozai's motivation; however, they accomplished the needed change of variables only through expansions, which limit accuracy. The reader is directed to Appendix A for the Hamiltonian expressions resulting from Vinti's method.

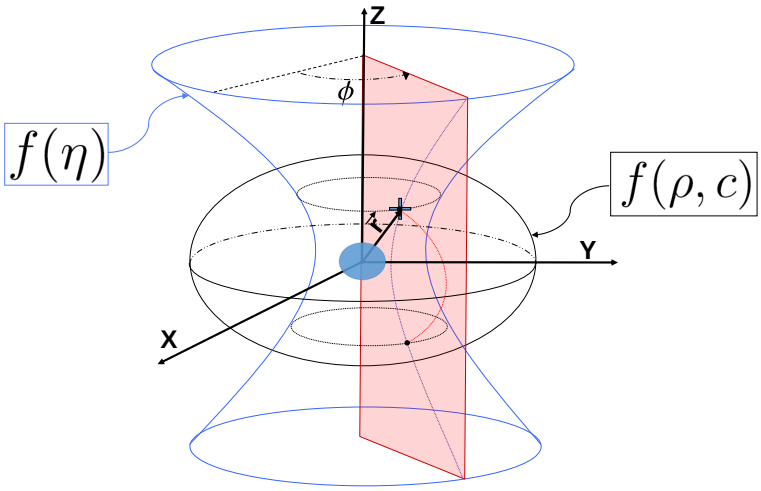

Figure 2.2: Vinti's Oblate Reference Frame

Although the solution was unique and elegant, difficulty arose with the inherent formulation and use of elliptical integrals in manipulating such a solution. These are found in the resulting generating function

$$W = \alpha_3 \lambda \pm \oint_{\rho^-} \frac{\sqrt{F(\rho, \alpha)}}{c^2 + \rho^2} d\rho \pm \oint_{\eta^-} \frac{\sqrt{G(\eta, \alpha)}}{1 - \eta^2} d\eta \tag{2.4}$$

where the integration contours ρ^- and η^- indicate integrating once around the orbit beginning at perigee and the southernmost point, respectively. Also, F and G are quartics of the form

$$F(\rho, \alpha) = c^2\alpha_3^2 + (c^2 + \rho^2)(-\alpha_2^2 + 2\mu\rho + 2(\alpha_1 + \omega_\oplus \alpha_3)\rho^2) \tag{2.5}$$

$$G(\eta, \alpha) = -\alpha_3^2 + (1 - \eta^2)(\alpha_2^2 + 2(\alpha_1 + \omega_\oplus \alpha_3)c^2\eta^2) \tag{2.6}$$

with α_i being the separation momenta. At the time, computing methods were inadequate at best for handling such expressions. Solving these elliptical integrals analytically encouraged the community to adopt the other seemingly viable and more usable solutions present at the time. [23]

This lack of interest did not discourage Vinti from continuing his attempts to solve and improve upon his solution. In 1961, he published the derivation of the theory and then somewhat of a recipe book for computing non-equatorial intermediary orbits using his solution [37; 38]. In 1962, he furnished a corollary to the previous papers by addressing equatorial orbits [39]. In 1963 he introduced a method to account for zonal perturbations to his solution [40]. These modifications were superseded in 1966 when he adjusted his original solution to account for the third zonal harmonic [41]. A subsequent improvement was released in 1969 but was structured very similarly to the recipe book of 1961 [42]. Using the new solution, he goes on to demonstrate how drag can be implemented using his unique variables [43].

The commonality in all the works presented here lies in the oblate spheroidal solution method. Accomplishing the change of variables required to separate the Hamilton-Jacobi equation is accomplished directly without expansions. Not only is this unique for orbital mechanics, it is remarkable considering that the full effect of J_2 and the majority of J_4 are included in the potential. However, the resulting equations of motion involving the infamous elliptical integrals are solved by expansions in J_2, thus reducing potential accuracy.

Recently edited in 1998, Vinti's published textbook furnishes the latest in attempts at a closed form solution to his problem posed almost 40 years prior [22:99-103]. However, these are still accomplished using expansions and thus introduce inaccuracies and unneeded complexities as opposed to solving the problem directly; doing so is demonstrated by Wiesel (see §2.7).

2.6 Works Acknowledging and Improving Vinti's Method

Since its publishing in 1959, the majority of authors who cite Vinti's solution acknowledge the elegance in such a formulation but quickly take a different tack due to the difficulties inherent in actually solving it. For instance, Barrar, in 1961, claims that "...Vinti's solution is undoubtedly an excellent one. However, Vinti only reduced the solution to quadratures. His result is four elliptic integrals of the third kind." He then proceeds to present a different method that ends up resembling Garfinkel's solution [44]. More recently, in 2012, Morrison even goes as far as to say that these resulting expressions result in "horrendous analysis, which we have pledged to avoid." [45:232]

A much smaller population are those who acknowledge the potential of using such a solution in an operational application. For example, Izsak starts with Vinti's "remarkable approximation" to earth's geopotential and attempts to perform perturbation theory to account for the difference between this and reality. The magnitude of this difference is on the order of J_2^2. His solution claims to account for J_2 through J_5, much like Brouwer's [46].

In 1964, Allen and Knolle take Izsak's formulation and develop a method of orbit fitting by calculating differential correction coefficients for least squares [47]. This approach is very similar to what will be presented in Chapter III. In 1967, Walden and Watson also applies differential corrections to this problem but focuses on Vinti's later modification in 1966 which includes the third zonal harmonic [48].

First in 1962 for the original solution, then again in 1966 for the inclusion of the third harmonic, Bonavito provides computational procedures for implementing Vinti's theory for computing an accurate reference or intermediary orbit [49; 50]. Then joining with others in 1969, he compares the theories of Brouwer and Vinti in accuracy and speed. To be clear, this Brouwer theory is the original one from 1959 and not the one blended with Kozai and

others to form SGP4. Bonavito's findings show that Brouwer's theory is "considerably less accurate" than that of Vinti [51].

Similar to Bonavito's comparison, Gordon et al examine differences between Brouwer and Vinti theory. However, they also consider Brouwer's solution as modified by Lyddane. They present results that confirm Vinti's superiority except for cross-track errors. They explain this is believed to result from the J_2^2 approximation for J_4, which is about 70% of the value. The work then presents a technique to perform a first-order general perturbations approach to account for this difference. After this change is made, results significantly improve. Cross-track errors are improved by more than 96% and in-track errors were reduced by 90% in certain orbits [52].

One of the few remaining modern day proponents of the Vinti theory is Gim Der. In 1996, he provided derivations and comparisons for Keplerian, Vinti, and numerical state transition matrices [53; 54]. Joining the likes of Bonavito, he edits Vinti's textbook in 1998 and provides an introduction applauding the "brilliant effort" of Vinti [22:viii]. Founding *DerAstrodynamics* in 2002, Der "...provid[es] innovative and specialized Astrodynamics algorithms for Space Situational Awareness applications" [55]. The theory of his algorithms and approach is rooted in Vinti's method.

With the exception of Der and Wiesel, Vinti's solution has more or less been forgotten. All the related efforts mentioned above use Vinti's method and the improvements thereafter as the basis for their research. The focus of the current research is to examine Wiesel's approach that results from modifying Vinti's original theory in 1959. His solution is, in every respect, a new one and should be treated as such.

2.7 Vinti's Problem As Modified By Wiesel

Wiesel takes Vinti's problem that has laid dormant for several decades and examines it through the lens of modern computing. Instead of posing that the elliptic integrals be performed analytically or through expansions, he offers they can be solved numerically.

Before giving the task to the computer, he manipulates the solution forms to avoid singularities and to provide more usable structures upon which to perform further beneficial calculations [23].

In solving Vinti's problem directly, Wiesel avoids expansions in J_2 that limited Vinti's potential accuracy when he attempted to solve his integrals analytically. Wiesel performs a change of variables to remove square root singularities in the elliptic expressions thus providing an avenue to furnish an obtainable numerical solution. Considering a quartic can be factored into its leading coefficient and roots as

$$F(\rho, \alpha) = A(\rho - \rho_1)(\rho - \rho_2)(\rho^+ - \rho)(\rho - \rho^-) \tag{2.7}$$

and introducing the change of variables illustrated in Figure 2.3 as

$$\rho = \frac{\rho^+ + \rho^-}{2} - \frac{\rho^+ - \rho^-}{2} \cos E_\rho \tag{2.8}$$

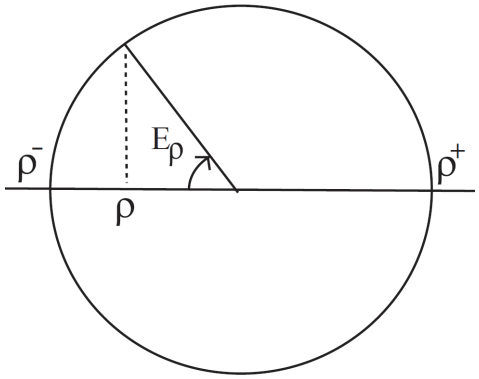

Figure 2.3: Circumscribing A Circle Between Integration Limits

Wiesel shows the square root factor of the quartic above (Equation 2.5) becomes

$$\sqrt{F(\rho, \alpha)} = \sqrt{A_\rho(\rho - \rho_1)(\rho - \rho_2)}\, |\rho^+ - \rho^-|\, |\sin E_\rho|/2 \tag{2.9}$$

where ρ_1 and ρ_2 are the roots that do not bracket the real trajectory and A_ρ is the coefficient of ρ^4. He repeats this process for $G(\eta, \alpha)$. In doing so, he generates two eccentric anomaly-like expressions for E_ρ and E_η requiring simultaneous computation. This new root finding method creates numerical difficulties at exactly equatorial (lacking a definite southernmost point) and circular (lacking a definite perigee point) orbits as well as near polar (argument of perigee rate is negative) orbits. Details of this are discussed in Chapter IV. These challenges could potentially be circumvented in the future through somewhat of a patch by reverting to Vinti's expansions in the neighborhood of such orbits. Providing such a fix is outside the scope of the current research but is recommended for future work.

Wiesel's process creates a new solvable problem from which to begin perturbations. He claims that this is "the other solvable problem." In comparison to the widely used two body problem, perturbations can begin on the order of 10^{-5} instead of 10^{-3}.

Not only is Vinti's solution separable but it can provide action-angle variables as promised by Hamilton-Jacobi theory. Having the generating function in hand, Wiesel demonstrates they can be found through performing a contour integral as

$$\mathcal{I}_i = \frac{1}{2\pi} \oint_{\Gamma_i} p_i dq_i = \frac{1}{2\pi} \oint_{\Gamma_i} \frac{\partial W}{\partial q_i} dq_i \tag{2.10}$$

where Γ_i is a contour around the torus encircling only one coordinate. To visualize this, consider a two dimensional system represented in phase space. Figure 2.4 shows this becomes a three dimensional torus in four space and how the integral goes around each coordinate separately.

For the quartic examined above, this expression looks like

$$\mathcal{I}_\rho = \pm \frac{1}{2\pi} \oint_{\rho} \frac{\sqrt{F(\rho, \alpha)}}{c^2 + \rho^2} d\rho \tag{2.11}$$

Separability of a system where time is independent indicates that each integral of the motion only depend on one variable and are therefore, uncoupled. Having access to the system's action-angle formulation provides valuable insight into periodic systems by

furnishing basis frequencies. Obtaining these frequencies using Hamilton-Jacobi theory has been termed Delauney's method [56:361-372]. Thus, the Delauney variables of orbital motion are the result of the two body problem being solved through such a process.

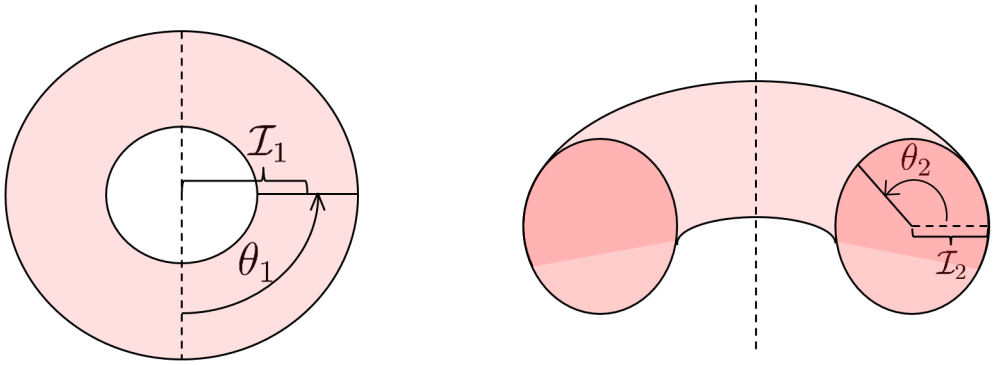

Figure 2.4: Contour Example: 2-torus in 4-space

Access to these valuable quantities is key to describing orbits on KAM tori. A brief introduction to KAM theory is offered in §2.8. Utilizing this theory will not be the emphasis of the current research, but using action-angles in a classical perturbation approach will be demonstrated for air drag in Chapters V and VI.

Duffy explores orbital resonances within Vinti's solution [57]. Using truth orbits for GPS satellites that sit on the 2:1 resonance, she examines stable, librational, and chaotic behaviors over different ten year trajectories. To avoid small divisors within the Vinti solution for these resonances, she presents a new transformation of variables.

A brief note on reference frames is in order. Wiesel performs an extra transformation in order to introduce a rotating reference frame. This sets the stage for using Vinti's solution to express orbits as lying on KAM tori. Since this is not the primary focus of the current research, $\omega_\oplus$ will be set to zero, thus providing an inertial frame [23].

2.8 KAM Theory

For perspective, a brief explanation and history of KAM theory is provided. First illustrated by Kolmogorov then later proved by Arnold and Moser (thus providing the theory's namesake), the KAM theory has mainly laid dormant in regards to orbital problems [58–61]. Introduced over 50 years ago, it offers that solutions for most lightly perturbed Hamiltonian systems lie geometrically on tori in phase space.

In the last decade, KAM theory has enjoyed a revival in being applied to modern orbital dynamics problems. The work of Celletti and Chierchia applies it to the Planar, Circular, Restricted Three Body system of the Sun, Jupiter, and the asteroid Victoria [62]. The remaining related works are predominantly by Wiesel and his graduate and post-graduate students at AFIT. These examine the theory as it applies to artificial satellites and comprise the majority of the literature with this purpose.

By taking the theory further, Wiesel suggests that earth-orbiting satellites lie on KAM tori [63]. This is a new and promising lens through which to view artificial satellite theory. The work by Little takes Wiesel's approach and attempts to compute tori on which actual satellites lie so that accurate positions are known [64]. Visher provides an independent verification of using tori for orbit propagation by comparing results to Systems Tool Kit (STK), as a truth model [65]. Further examination of various methods to construct a torus through new spectral methods is preformed by Wiesel and Bordner [66; 67].

Craft explores the utility and viability in planning for satellite constellations to exist on the same torus, only separated by angle displacements. The benefit here is the near constant formation separation reducing fuel allowance for constellation station-keeping[68]. Yates explores the compensation errors in reference tori for effects due to air drag and third body perturbations [69]. Hagen goes on to examine these effects as it applies to KAM theory and shows that the theory still holds in the presence of these light perturbations [70]. Dunk

applies lessons and methods learned earlier to the unique environment of highly eccentric orbits [71].

Frey demonstrated extracting KAM torus basis freqencies from SGP4 and two-line elements sets (TLE). However, this method is problematic at low eccentricity [72]. Using Wiesel's new theory for nearly circular orbits [73], Abay performs orbit fitting by constructing KAM tori based on TLEs, of orbits with low eccentricity. When compared to SGP4 fits for the same orbits, results are up to 5 times better [74].

This review of literature relating to and applying KAM theory to artificial satellite motion is not all inclusive. It does, however, highlight the emergence of modern applicability and practicality to a theory that has yet to be fully recognized. Although results are promising, these earth-orbiting tori methods are, in a fashion, disconnected from the actual theory. This is true because they do not utilize the original method used to prove the theory. That method uses a canonical transformation between two systems that exist in action-angle coordinates. So, the original system must possess a full range of frequencies, termed non-degenerate. The typical approach in perturbation theory is to use the two body problem as the original system, which is fully degenerate since two of the three fundamental frequencies are zero. Thus, this does not contain any range of frequencies and is therefore not acceptable. So, in these techniques, near realistic orbits were simulated or actual data was received and frequencies were extracted after the fact through various spectral methods [23].

Unlike previous attempts, using Vinti's solution as a starting point is encouraging in that it produces the full range of frequencies needed to perform necessary canonical transformations. The promise of frequencies is due to the perturbing zonal harmonics accounted for therein. Thus, having those frequencies as a result of the solvable solution allows for perturbation theory to be applied with respect to these frequencies. The significant benefit in such a demonstration is the potential to easily model long term

behavior of the motion due to highly accurate basis frequencies. Slight frequency inaccuracies exist in modern OD software, such as SGP4, which tends to a divergent solution after a period of time. However, if the frequencies can match the dynamics solution, the current position error will not grow with time but will slightly oscillate around the truth within a reasonable margin.

2.9 Summary

With the growth of orbital debris and the expected significant increase of catalogued items, accurate analytical solutions should be sought after with the fervor in which they were in the late 1950s. Complacency in traditional methods has the potential for catastrophic results by creating millions of conjunction warnings when only two or three require attention. The stage is set to explore other avenues with which to pursue advancement in this field. What follows is an examination of one of these options. The solution used is only at the beginning of its development but will be demonstrated to already compete with SGP4 in a perturbation-limited comparison. A method to begin adding perturbations to this solution is explored by accounting for the next largest effect past the geopotential, air drag.

III. Orbit Fitting

This chapter details how the current research will leverage the newly revised Vinti solution in an orbit fitting scheme. A nonlinear least squares algorithm is implemented for differential correction of a reference or estimated orbit based on provided observations. This method uses the Vinti state transition matrix that is found through finite differencing techniques. Validation of the matrix calculation and initial fitting performance is provided.

3.1 Using Nonlinear Least Squares

Among the various estimation techniques available, the current research will utilize the capabilities of a batch method, nonlinear least squares routine to perform orbit fitting using a set or "batch" of observations. Benefits inherent in least squares that are attractive for the current research include simplicity, stability, and speed. On the other hand, Kalman filters would be best suited for sequential estimation of stochastic or random components of a dynamics or measurement model where the prediction is improved upon continuously with each piece of new data.

This research hopes to minimize the amount of random behavior and drill down to the core of a Vinti model examination. When considering orbital motion, the main perturbing effects that are the least predictable include those of atmospheric fluctuations (to be discussed in Chapter V) due to solar activity and the like. Further, a batch method is used to mimic how JSPOC performs orbit fitting. Observations worldwide for a specific catalog item are processed each time a specific, analytical orbital solution is improved upon.

A more rigorous derivation and statistical treatment of this method can be found in Vallado [27:728-753] and Wiesel [75:60-73]. What follows describes the relevant aspects

of the overall algorithm. Key summaries are included here for clarity and to identify necessary quantities.

3.1.1 An Introduction

We begin with a system whose dynamics are shown as equations of motion

$$\dot{\mathbf{X}}(t) = \mathbf{f}(\mathbf{X}, t) \tag{3.1}$$

to be numerically integrated or as an explicit solution

$$\mathbf{X}(t) = \mathbf{h}(\mathbf{X}(t_0), t). \tag{3.2}$$

where $\mathbf{X} = (x, y, z, \dot{x}, \dot{y}, \dot{z})^T$. This nonlinear mapping in Equation 3.2 best represents the Vinti solution: one directly obtains the state $\mathbf{X}$ at some time t, given the state at time t_0. The dynamics of the orbital motion are assumed to be deterministic without random noise. However, as is the fundamental requirement for all estimation techniques, the true states are unknown and must be estimated.

In this method, a reference trajectory is required. State estimates calculated from this *guess* of an orbit serve as predictions for where we believe the satellite will be at some time in the future. The goal of our estimation scheme is to modify this reference orbit to be as close to reality as possible.

To begin, a state vector at some epoch time is needed to describe this orbit. In catalog maintenance, this reference trajectory results from a previous orbit fit, perhaps one day or one week in the past. The current batch of data to process represents all observations received since the last fit. Characterizing maneuvers of active satellites that have occurred since the last fit or other external circumstances is outside the of scope of the current research.

From the perspective of catalog maintenance, the state at epoch can be taken from a previous fit. For an uncorrelated track, or observations from an orbit that does not readily line up with another cataloged item, this reference guess is generated using some initial

determination scheme. This can be a complex process and will not be covered here. It is then corrected to result in a trajectory that is satisfactorily close to the truth.

Deterministic dynamics allows for the expression

$$\delta\mathbf{X}(t) = \Phi(t, t_0)\delta\mathbf{X}(t_0) \tag{3.3}$$

to be valid, where $\delta\mathbf{X}$ is some small variation to the state. $\Phi(t, t_0)$ is termed the state transition matrix and is a Jacobian matrix containing partials derivatives of the state $\mathbf{X}$ at time t with respect to the state at time t_0, to be found later (see §3.1.5.1). This allows us to say that some small displacement at time t_0 can be propagated to some time t. Effectively, this shows us how the state at time t will be affected by a minor adjustment at the epoch time. This concept becomes important when we try to minimize the difference between our predicted orbit and the one being observed.

A numerically integrated orbit serving as a truth model (see §3.1.3) generates a batch of observations, $\mathbf{z}$, to be used in fitting. This $\mathbf{z}$ vector is usually related to the state vector through some nonlinear function $\mathbf{G}(\mathbf{X})$. To simplify analysis, this relationship will be one to one with the position vector of the truth orbit or $\mathbf{z} = \mathbf{G}(\mathbf{X}) = (x, y, z)^T_{truth}$. Therefore, no complex linearizations or observation relationships are needed. Also, weights that account for noise expected in the measurement will not be used but could easily be incorporated for realistic applications. The general process follows.

3.1.2 The Algorithm

Derivation of the linear form of least squares gives the normal equation

$$\mathbf{X}(t_0) = (T^T Q^{-1}\, T)^{-1}\, T^T Q^{-1}\, \mathbf{z} \tag{3.4}$$

where one can directly solve for the state given a set of observations. Note that the matrices on the right are accumulated values and the $\mathbf{z}$ vector contains all measurements from the batch. However, with the high nonlinearity of the problem, it is necessary to solve for corrections to a predicted orbit based on residuals. This equation is identical in form after

these quantities are exchanged

$$\delta\mathbf{X}(t_0) = (T^T Q^{-1}\ T)^{-1}\ T^T Q^{-1}\ \boldsymbol{r} \tag{3.5}$$

Above, Q represents a weighting matrix that can account for noisy measurements. T is the linearization of the measurement multiplied by the state transition matrix and can be found as

$$T = H\Phi(t, t_0) \tag{3.6}$$

where

$$H = \frac{\partial \mathbf{G}}{\partial \mathbf{X}} = \begin{bmatrix} 1 & 0 & 0 & 0 & 0 & 0 \\ 0 & 1 & 0 & 0 & 0 & 0 \\ 0 & 0 & 1 & 0 & 0 & 0 \end{bmatrix} \tag{3.7}$$

Since no process noise will be added to the measurements, Q will be taken as the identity matrix. However, it will remain in the explanation below for generality.

A step-by-step explanation of the iterative process will now be provided as well as a flow diagram, see Figure 3.1. Given an initial guess of the epoch position and velocity defining the reference orbit, perform the following for each observation time, t_i, for all n observations:

- Using the Vinti package[7], produce a state estimate and calculate the state transition matrix, $\Phi(t_i, t_0)$
- Subtract the predicted position from the observed state producing the residual vector $\boldsymbol{r}_i = \mathbf{z}_i - H\mathbf{X}_{i,predicted}$
- Accumulate values to running sums of the matrix

$$\sum_{i=0}^{i} T_i^T Q_i^{-1}\ T_i \tag{3.8}$$

[7] *Vinti package* refers to the set of routines that calculates Vinti's solution as modified by Wiesel. It inputs a state vector at some epoch time and outputs various orbital parameters at some other specified time.

and the vector

$$\sum_{i=0}^{i} T_i^T Q_i^{-1} \boldsymbol{r}_i \tag{3.9}$$

After all n observations are processed (when $i = n$),

- The correction to the reference orbit can be calculated as

$$\delta\mathbf{X}(t_0) = \left(\sum_{i=0}^{n} T_i^T Q_i^{-1} T_i \right)^{-1} \sum_{i=0}^{n} T_i^T Q_i^{-1} \boldsymbol{r}_i \tag{3.10}$$

- Correct the reference orbit

$$\mathbf{X}_{ref'}(t_0) = \mathbf{X}_{ref}(t_0) + \delta\mathbf{X}(t_0) \tag{3.11}$$

- If convergence criteria is met, the process is complete with $\mathbf{X}_{ref'}$ being our best estimate of the true orbit. If not, begin again to successively calculate corrections. Convergence criteria is unique to each application but is essentially a way to determine when the estimation routine has exhausted its ability to find a better solution. Using a parameter to indicate *goodness* of a fit, Root Mean Square (RMS, to be explained shortly) can be compared between iterations to see if the solution is improving and if the routine should continue. Determining the percentage change, criteria to quit can be set with

$$\left| \frac{RMS_{old} - RMS_{new}}{RMS_{old}} \right| \leq \epsilon \tag{3.12}$$

  Convergence during this research was typically declared after only 3 or 4 iterations while maximum iterations were set to 10. Setting a maximum number is a second way to decide when to quit by admitting that the solution will not improve by simply repeating the process endlessly.

- Examine and analyze residuals.

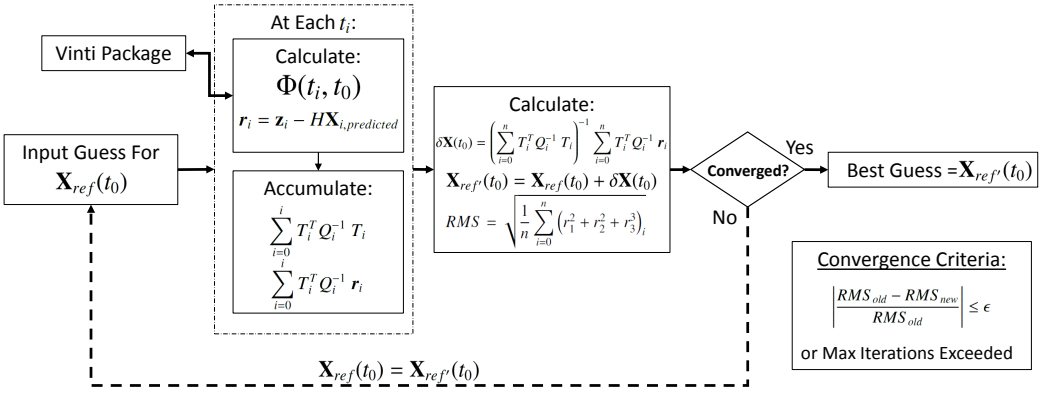

Figure 3.1: Iterative Nonlinear Least Squares Fitting Routine

A Root Sum Square (RSS) of the residuals can be used to plot and visualize model divergence, or error growth, over time. With this, the three components of the residual vector for each observation are squared, summed, then the square root is taken. This looks like

$$RSS_i = \left(\sqrt{r_1^2 + r_2^2 + r_3^3}\right)_i = |\boldsymbol{r}_i| \tag{3.13}$$

This represents the magnitude of the estimated error at that time. Then, for n observations, these values can then be averaged over the entire fit to give an average error,

$$RSS_{avg} = \frac{1}{n}\sum_{i=0}^{n}|\boldsymbol{r}_i| \tag{3.14}$$

Root Mean Square (RMS) error is the basis for least squares methods due to its numerical stability and speed. Residual components are squared and summed for each observation. When this is complete for all observations, the mean is taken and then the

square root as in

$$RMS = \sqrt{\frac{1}{n}\sum_{i=0}^{n}\left(r_1^2 + r_2^2 + r_3^3\right)_i} \tag{3.15}$$

This is computationally more efficient than RSS because the square root operation is required only once at the end of data accumulation as opposed to once every observation. RMS can provide a snapshot of fit performance although it is not the mathematical average error. In practice, RMS and RSS values are similar in magnitude and are related by

$$RMS = \frac{1}{\sqrt{n}} RSS_{avg} \tag{3.16}$$

3.1.3 Truth Model

Before moving on with the development of the fitting routine, a description of the truth model is in order. A numerical integration routine using a fourth-order predictor corrector algorithm is used. It uses a Hamming integrator that is known for stability and speed. Flexibility is inherent with this tool as various geopotential scenarios can be implemented. For instance, a zonals only or full geopotential (to specified order and degree) can be declared. Unique to the current research, a Vinti geopotential can also be invoked simulating the exact potential that is accounted for in Vinti's solution. This is used in initially validating the fitting scheme and later in comparing drag-only perturbation methods. In Chapter V, the process of using this truth model to estimate air drag effects will be explained.

3.1.4 Dimensionless Units

When using orbital velocities and distances, units can be problematic. For example, if metric units are desired a low earth satellite may have a radius vector on the order of 7000 km with a velocity of 6 or 7 km/sec. Maneuvers or changes in velocity would be on the order of centimeters or meters per second. Numerical conditioning can quickly become an issue when dividing a large number by a very small number.

This research will utilize geocentric dimensionless distance units (DU) and time units (TU). These result from scaling position and time relative to the size and rotational speed of the earth. DUs are calculated by dividing by the average radius of the earth. For metric units, this means 1 $DU \approx 6378.1363$ m. TUs are found by determining the speed at which an object would orbit the center of the earth from this average radius but at the equator. This is found by the expression $\frac{TU}{sec} = \sqrt{\frac{\mu}{Re^3}}$ and μ is earth's gravitational constant multiplied by its mass. This works out to be 1 $TU \approx 806.81$ sec. Using these nondimensionalized units results in orbital parameters on the order of unity which is preferred for numerical reasons.

3.1.5 State Transition Matrix

Obviously, with the estimation approach laid out above, finding the partials matrix or state transition matrix using Vinti's dynamics is critical. The information provided by the Phi matrix can be visualized as providing the slope of the solution space around the reference orbit with which to modify it, creating a more accurate orbit fit. Considering the numerous changes of variables and chain rule operations associated with taking these partial derivatives analytically, they are performed numerically. This approach is called finite differencing and is not uncommon especially with rapid analytical propagators. Vallado says the time and money needed to develop elegant analytical solutions is most likely not worth the slight overhead needed to simply go ahead and calculate them through numerical partial differentiations [76].

3.1.5.1 Finite Differencing

The matrix of interest is a Jacobian and can be displayed as

$$\Phi(t, t_0) = \frac{\partial \mathbf{X}}{\partial \mathbf{X}_0} = \begin{bmatrix} \frac{\partial x(t)}{\partial x(t_0)} & \frac{\partial x(t)}{\partial y(t_0)} & \cdots & \frac{\partial x(t)}{\partial \dot{z}(t_0)} \\ \frac{\partial y(t)}{\partial x(t_0)} & \frac{\partial y(t)}{\partial y(t_0)} & \cdots & \frac{\partial y(t)}{\partial \dot{z}(t_0)} \\ \vdots & \vdots & \ddots & \vdots \\ \frac{\partial \dot{z}(t)}{\partial x(t_0)} & \frac{\partial \dot{z}(t)}{\partial y(t_0)} & \cdots & \frac{\partial \dot{z}(t)}{\partial \dot{z}(t_0)} \end{bmatrix} \tag{3.17}$$

First, the reference orbit is used to generate several other orbits using finite displacements in each direction of the position and velocity at the epoch time. This is repeated for $-\delta X_i$, $+2\delta X_i$, and $-2\delta X_i$ for a total of 24 additional orbits. These displaced orbits are then run through the Vinti solution package resulting in position, velocity vectors at the observation time. Figure 3.2 illustrates this process and Figure 3.3 shows what this would look like in configuration space for three position displacements.

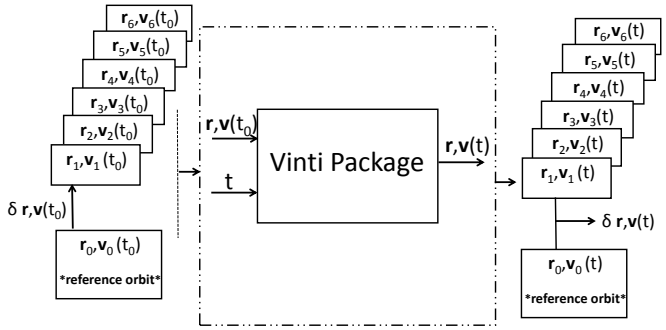

Figure 3.2: Construction of Nearby Orbits

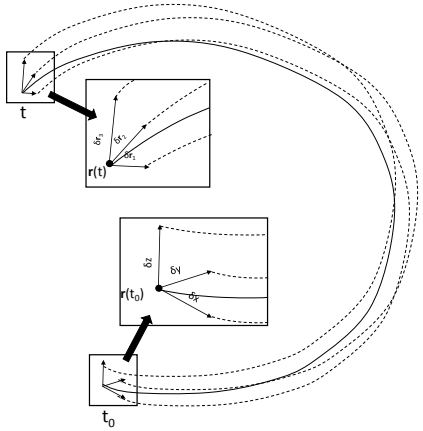

Figure 3.3: Visualization of Three Nearby Orbits (Configuration Space)

The elements of the Phi matrix are then calculated following

$$\frac{\partial f}{\partial x}(x) \approx \frac{1}{\Delta x}\left(\frac{1}{12}f(x-2\delta x) - \frac{2}{3}f(x-\delta x) + \frac{2}{3}f(x+\delta x) - \frac{1}{12}f(x+2\delta x)\right) \tag{3.18}$$

a five point Lagrangian partial derivative [77:25.3.6]. This method can be likened to how an Unscented Kalman Filter samples a system's nonlinearities directly, avoiding linearizing the dynamics in the partials matrices. When nonlinear effects become large for certain orbits, an added performance boost may be expected by avoiding linearization errors.

The magnitude of the position displacements is determined by taking the magnitude of the position vector, in DU, and multiplying by 10^{-5}. The same process is accomplished for velocity displacements relative to the velocity vector, in DU/TU. This value was chosen so it makes the position and velocity state displacements on the order of 75 m and 7.5 cm/sec, respectively. Using these dimensionless parameters, this requires 5 or 6 significant figures and with double precision, there are digits to spare. Any larger and there would not be sufficient granularity required to fully characterize the orbit. Any smaller and there would be risk of round-off error. Further, using geocentric, nondimensionalized units of DU and TU avoids numerical problems encountered when dividing large astronautical distances by small velocities.

3.1.5.2 Validation

To ensure the state transition matrix at hand is usable and accurate, it must be validated. Using linear systems theory, the Phi matrix follows certain properties. First, if the predicted time equals the epoch time, the result is

$$\Phi(t_0, t_0) = I \tag{3.19}$$

Next, the change in behavior over time should follow

$$\dot{\Phi} = A\Phi \tag{3.20}$$

where A is a 6x6 matrix and when broken down into the four 3x3 sub-matrices looks like

$$A \approx \left[\begin{array}{c|c} \emptyset & I \\ \hline A_{2,1} & \emptyset \end{array}\right] \tag{3.21}$$

$A_{2,1}$ contains the gravitational acceleration terms. The upper right block should be an identity matrix due to state space relation between position and velocity. The diagonal blocks should be nulls as a result of absence of these terms in the equations of motion.

To test this structure, an incremental predicted time supplied, or $\Phi(\delta t, t_0)$ should result in the form

$$\dot{\Phi} = \frac{\Phi(t_0 + \delta t) - \Phi(t_0)}{\delta t} = AI \tag{3.22}$$

These checks were performed adequately where the resulting matrices were of the necessary structure.

Next, an idea of how long the difference approximation of the Phi matrix would be valid is examined. For this, a truth model Phi matrix was used for comparison. In the numerical integration truth model used, the capability exists to also integrate Equation 3.20 above. The matrices from both models were calculated incrementally over a period of time and compared. At each time step, the difference was taken creating what can be termed a del matrix. Various norms[8] were then taken on this del matrix and plotted over time. This was performed for a certain size and inclination of orbit[9] and then repeated over various eccentricities. Results from a few of these are shown in Figures 3.4 to 3.6.

The Phi matrix as found through finite differentiation seems to remain within a reasonable margin of the integrated one over a two day span. As illustrated, some errors oscillate within the same tolerance and others grow apart over time. Either way, the value of the difference is less than 6% over the time examined except for when eccentricity approaches 0.9. Considering the time periods of interest in orbit fitting and the purposes

[8] 1-norm: Max column sum; Frobenius norm: Square root of the sum of the square of all elements; Infinity-norm: Max row sum

[9] altitude at perigee: $\approx 3,500$ km, inclination: 20^o

of this research, the Phi calculations are implemented appropriately to be inserted into the fitting routine. The Phi quantities will still provide the slope in solution space for convergence, however quadratic convergence, common in least squares estimation, may be lost and require more iterations to complete the routine.

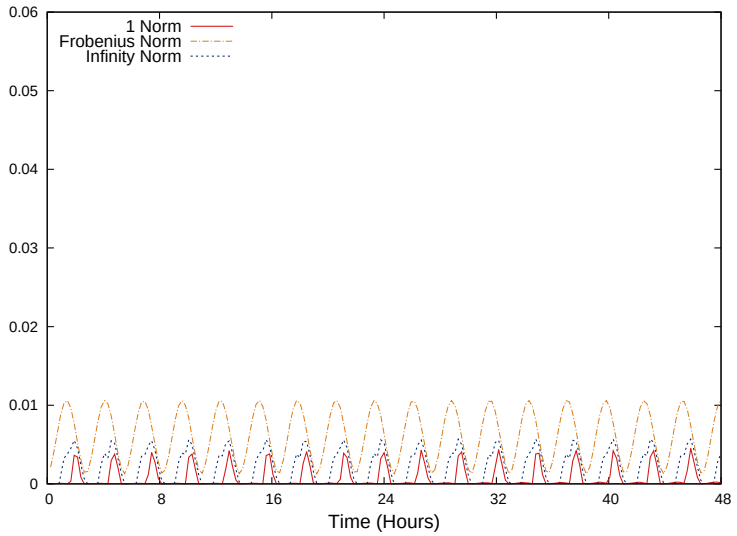

Figure 3.4: Norms of Phi Difference: e = 0.001

3.2 Initial Orbit Fitting Performance

With the Phi matrix available and validated, the least squares orbit fitting scheme can be tested. As an initial check of the model and code, sample observations from a trajectory perturbed only by Vinti's geopotential[10] are created every minute for one day and supplied to the Vinti OD software. This limited perturbation approach allows for an initial comparison between truth and estimation methods by keeping the observation perturbations equal to those accounted for in Vinti's solution. The only differences should be numerical and can help characterize errors in the model or calculations.

[10] zonal potential terms past J_2 are approximated as $J_4 = -J_2^2$, $J_6 = J_2^3$ and so on

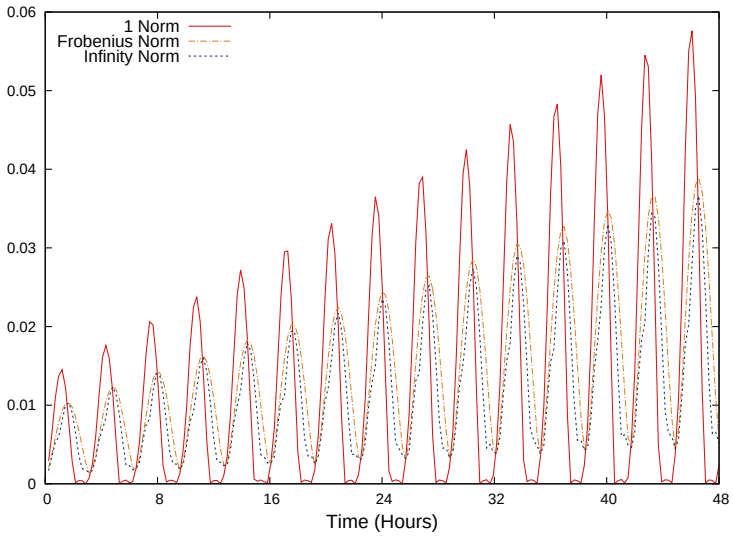

Figure 3.5: Norms of Phi Difference: e = 0.1

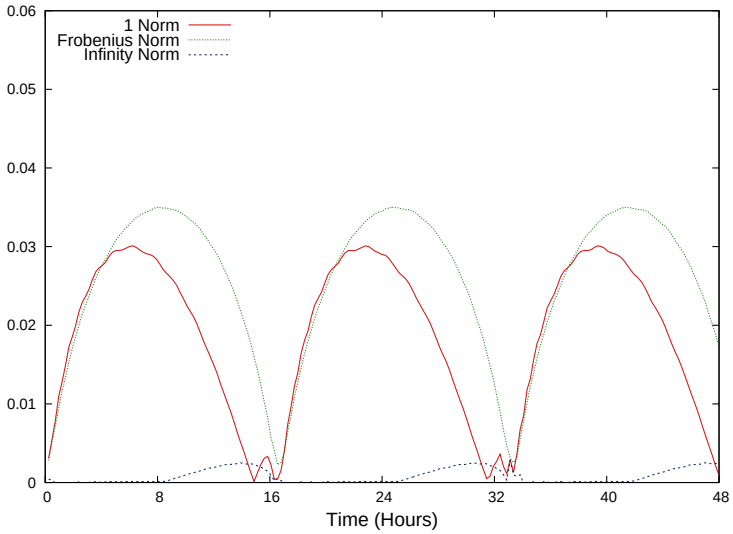

Figure 3.6: Norms of Phi Difference: e = 0.7

Five sample orbits with various parameters were created and fit using the above methodology. Results are summarized in Table 3.1. As expected, performance varies depending on size and shape of the orbit. However, centimeter-level fits provide confidence

that the dynamics model, Phi calculations, and fitting mechanisms are working in concert as expected. Wiesel's advertised error is commensurate with these magnitudes [23].

Table 3.1: Vinti Geopotential Orbit Fits

Test Orbit	Perigee Altitude (km)	e	i	RMS (cm)
1	400	0.01	28.5^o	29.5
2	500	0.2	45^o	20.8
3	800	0.2	28.5^o	17.9
4	1000	0.7	28.5^o	74.6
5	1000	0.001	0.01^o	9.8

To provide more insight into the RMS values, residuals over time are shown for the first two orbits in Figures 3.7 and 3.8. These illustrations decompose where the errors manifest, allowing understanding into how the model fails to match reality. Again, as expected, these differences seem to be a function of the size and shape of the orbit. There appears to be a bias in the radial direction for all orbits tested. This bias is speculated to result from a period compensation. Adjusting radial position by the model is the most direct way to make up for inaccuracies in modeling the orbital period. However, for Orbit 1 (Figure 3.7), there appears to be a more pronounced difficulty in matching the period as evidenced by the linear growth on either side of the midpoint of the radial and in-track residuals. Otherwise, the residuals seem to exhibit stable behavior and can possibly be explained by noise in the calculations. Noise on the centimeter level is acceptable considering it is on the order of solution error. Three other orbits are analyzed and similar figures can be found in the appendix for reference.

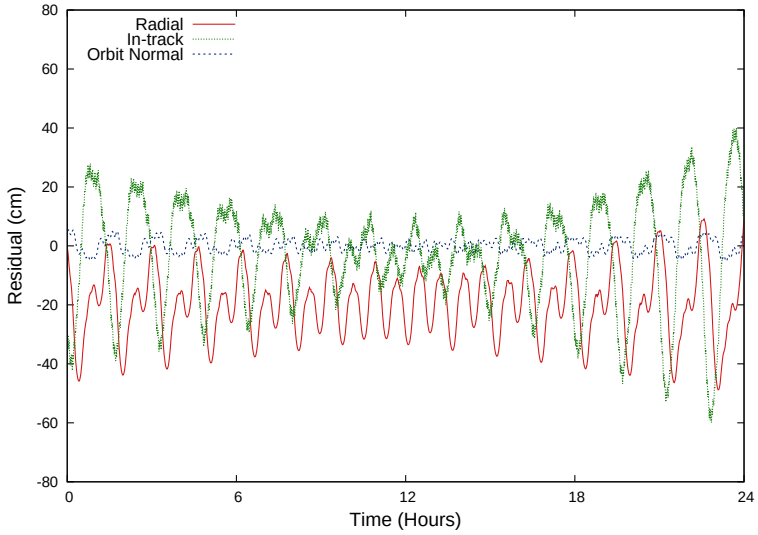

Figure 3.7: Vinti Geopotential Fit Residuals: Orbit 1

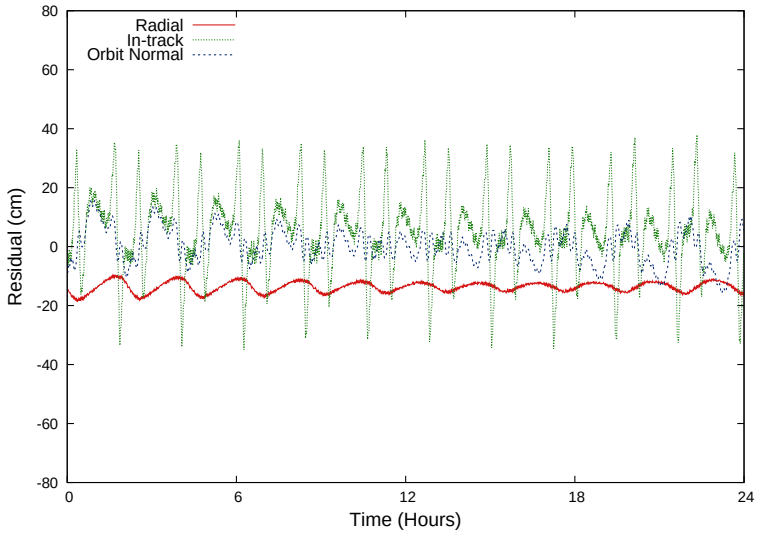

Figure 3.8: Vinti Geopotential Fit Residuals: Orbit 2

3.3 Conclusion

This chapter demonstrated the orbit fitting method for the current research to include finding the state transition matrix. Preliminary checks provide confidence in the

implementation and development of computer code to perform needed calculations for further analysis. Initial performance of the fully implemented fitting procedures lays the foundation upon which to examine how well the Vinti solution can approximate the full geopotential and effects due to air drag.

IV. Results

This chapter reviews the performance of the Vinti fitting routine as developed in Chapter III when used to fit orbits perturbed by the full geopotential. A wide survey of fit performance is taken across various inclinations and eccentricities. Next, a detailed analysis is given for two representative orbits. These demonstrations help identify best case and worst case behavior within a functional orbital regime for this solution. These same example orbits are then used for an exercise in predicting future miss distances.

4.1 Fitting Performance

Following the procedure explained in Chapter III, truth observations are created once every minute for one day using different sizes and shapes of orbits. Unlike earlier, these orbits are perturbed by a full, 20x20 geopotential. For added perspective, these orbits are also provided to a least squares fitting routine using an unclassified version of SGP4. Using the same test orbits from Table 3.1, Table 4.1 shows the resulting RMS values. Again, RMS indicates *goodness* of a fit.

Table 4.1: RMS Values For Full Geopotential Orbit Fits (m)

Test Orbit	Vinti	SGP4
1	603	500
2	220	878
3	245	982
4	108	5154
5	458	458

At first glance when comparing RMS values, Vinti seems to outperform SGP4, however, it should be noted that SGP4 is at a slight disadvantage. The truth observations are only perturbed by a full geopotential, while SGP4 is attempting to incorporate *all* perturbations with the exception of air drag. This disconnect becomes more prominent when the apogee of an eccentric orbit is high enough for third body effects to be noticeable, Orbit 4 for example which reaches an altitude of over $35,000$ km. Therefore, this does not provide an ultimate performance comparison between the two models. What it does provide, though, is some relative metric from which to draw some inference. In the future, these additional perturbations could be added to the solution for a more accurate representation of reality.

Even considering the disadvantage of a slight mismatch of perturbations, the fact that the Vinti model is mostly doing better than SGP4 is promising. The geopotential is the dominant perturbation in these low earth orbits. SGP4 is at an end when approximating for these effects by truncating after expansions through J_5. However, the Vinti model is only using the solvable solution which accounts exactly for J_2 and nearly three-fourths of J_4. The true test will be when the remaining geopotential effect is incorporated through a general perturbations approach. This is left for future works.

4.1.1 A Wide Survey of Orbits

Before detailed information of any one orbit is presented, a wide range of orbits is sampled. This gives an idea of relative best case/worst case scenarios while illustrating where the model works and where it struggles. Figure 4.1 shows a sampling of eccentricities and inclinations for a perigee height of 400 km.

It is evident the Vinti solution as modified by Wiesel begins to break down for inclinations greater than 60^o or so. However, this is not as a result of any critical inclination difficulties in the sense of singularities resulting from a zero apsidal rate. All data indicates singularities do not exist at or near 63.4 as there does in other theories such as Brouwer's

original solution. These errors seem to grow to infinity when approaching the polar regime. When increasing inclination, an RMS of around 25 km was calculated at 82.5^o. When decreasing inclination towards polar, similar RMS was found at 97.5^o. A solution does not exist between due to a numerical flaw in the Vinti integrals. Resolving this flaw is outside the scope of the current research.

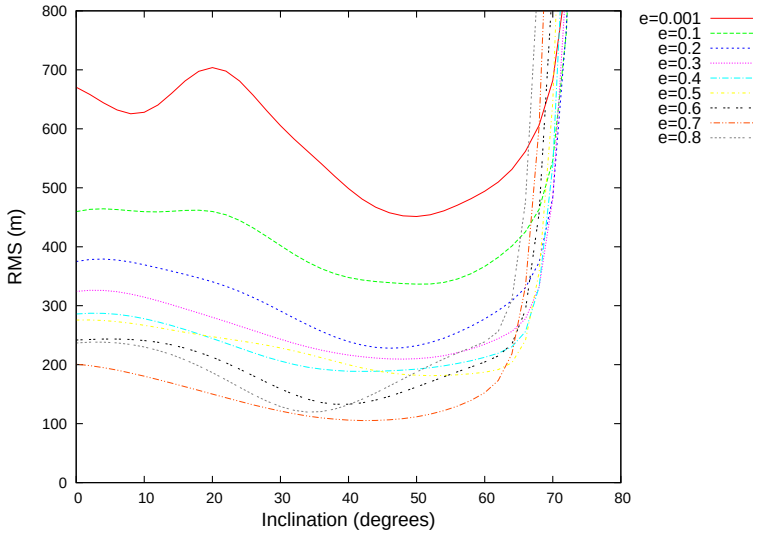

Figure 4.1: Orbit Fit Performance: Perigee Height = 400 km

When inclination is increased past polar, the errors eventually come down and behavior begins to resemble what it was at inclinations below the first critical inclination. This occurs near the *other* critical inclination which is about 116.6^o (for reference, the critical inclinations are noted on Figure 4.2 with blue arrows and the reader is directed to Appendix C for more details on the critical inclination phenomena). The argument of perigee is fixed in inertial space at these two locations but apsidal rate is negative between them. It is the author's belief that this negative rate is the source of the numerical flaw within the Vinti integrals as modified by Wiesel.

Vinti's original solution was claimed to be accurate through high inclination. This means a negative rate should not have been an issue. The difference is suspected to manifest

in Wiesel's root finding scheme illustrated in §2.7. To solve for some of the terms in his elliptic integrals numerically, he integrates from perigee to apogee. Therefore, if this negative rotation is not accounted for properly, a less accurate solution, and ultimately a singularity, could be the result.

Singularities do exist for equatorial and near polar orbits as well as eccentricity of zero. Vinti's original theory did not have such problems but Wiesel's numerical solving routine relies on certain root finding methods that need a definite perigee and northernmost point. However, eccentricities as low as 0.001 and inclinations of 0.01 have resulted in satisfactory fits. Detailed analysis for performance of this fitting routine will focus on a functioning orbital regime of non-circular orbits in the inclination range of greater than 0^o but less than 65^o.

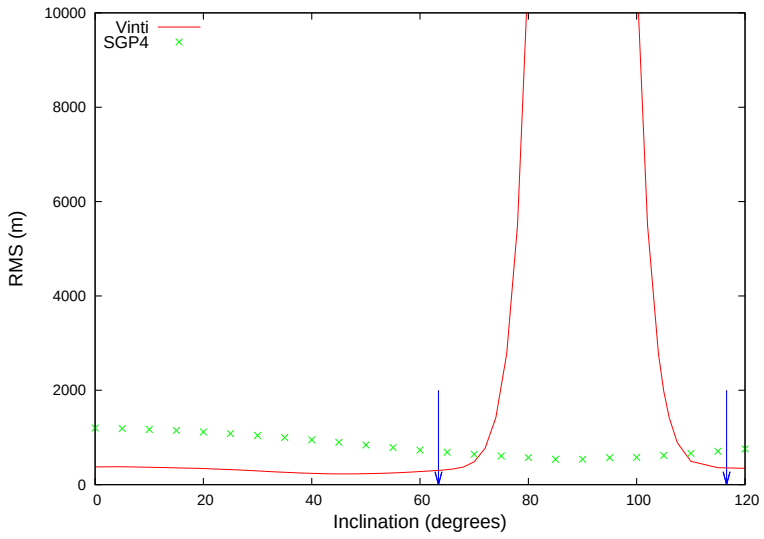

Figure 4.2: High Inclination Issue: Perigee Height = 400 km, Eccentricity = 0.2

4.1.2 A Closer Look

When comparing data from Table 4.1 and Figure 4.1, there are noticeable variations in performance for different orbital parameters. The first two test orbits in the table are identified as candidates for further analysis. They are used because they seem to represent

a worst case (Orbit 1) and best case (Orbit 2) scenario from the functional range of inclinations with a reasonable eccentricity of 0.2 or lower.

Figure 4.3 displays residuals for the one day fit. Since the observations are created from the truth model with no process noise, the residuals are actually the error. These terms will be used interchangeably.

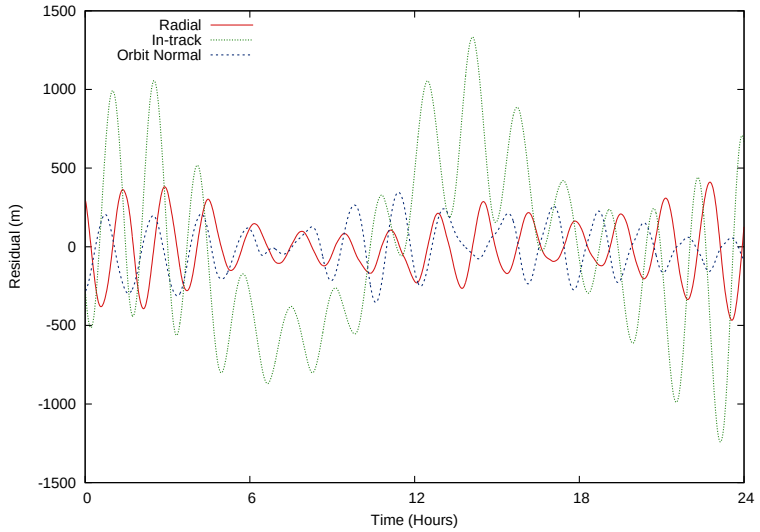

Figure 4.3: Full Geopotential Fit Residuals: Orbit 1

Notice all the residuals exhibit a periodic behavior that coincides with the orbital period. In addition, the in-track error has an extra, longer oscillation with a period of about half of a day. For orbit 1 which has an RMS of 603 m, Table 4.2 shows more detailed statistics about this fit. Considering the scale, all the errors are near zero mean so there is no bias within the day fit. When the data is fit to a normal distribution, the standard deviation, σ, illustrates how spread out the errors are. This combined with the minimum and maximum errors show the in-track errors are by far dominant. This artifact was also illustrated by Gordon in 1978 when he compared Vinti, Brouwer, and Brouwer-Lyddane solutions [52].

Table 4.2: Error Statistics From Orbit 1 Fit (m)

	Average	σ	Min	Max
Radial	-4.6	180	-467	411
In-track	0.03	554	-1241	1334
Orbit Normal	-5.9	152	-355	347

Orbit 2 is a much better fit with an RMS value of 220 m. Figure 4.4 shows a similar periodic trend but the longer frequency error is less pronounced in-track. Again, Table 4.3 shows that means were near zero and the error in the velocity direction was the greatest contributor to overall error.

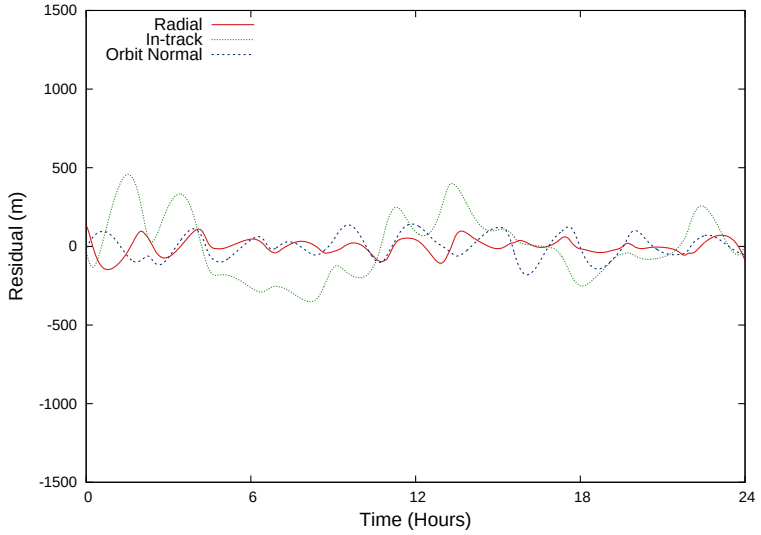

Figure 4.4: Full Geopotential Fit Residuals: Orbit 2

4.2 Error Growth

Wiesel's solution at the heart of a fitting routine has displayed initial promise for adequate results for a certain range of orbital parameters. It is, at the least, comparable

Table 4.3: Error Statistics From Orbit 2 Fit (m)

	Average	σ	Min	Max
Radial	-1.3	50	-147	126
In-track	-0.2	201	-353	456
Orbit normal	2.6	76	-181	141

to how SGP4 performs when fitting the same data. However, fitted data is in the past and potential collisions are in the future. Therefore, an orbital propagator is only as good as how well it can fit an orbit then predict a future position/velocity state. This, combined with other fits and predictions, provide miss distances for nearby orbiting craft or debris.

An idea of how long a solution will be valid is explored. Data is fit for one day then used to predict future positions. This is compared to what the integrated truth model outputs for those future times using the same orbit. Orbits 1 and 2 from above are examined again in this exercise.

After the magnitude of the position error at each timestep is calculated, Figures 4.5 and 4.6 show the behavior in future predictions as compared to the integrated truth. Notice the difference in scale between the two. In both cases, an increasing amplitude periodic error exists while a secular growth is evident. When considering geopotential effects, even zonal terms contribute to periodic changes in semi-major axis and eccentricity, secular growth in the node and argument of perigee, and a combined secular/periodic effect on mean anomaly. However, sectoral and tesseral contributions are only periodic for all the elements. The approximation of even zonals beyond J_2 and lack of the remaining sectoral/tesseral terms can be implicated by this error growth behavior.

When a linear fit is calculated for the future error, the slope of that line is a good estimate of the average error growth rate. For the worst case, Orbit 1, the average growth is a little over 1 km per day. For the best case, Orbit 2, the error growth is estimated to be

about 370 m per day. This difference can lend insight into how well a day's fit will translate into future error growth. Since these two sample orbits seem to bound the performance within usable orbit regimes, it could be inferred that average error growth for other orbits should lie between these two values.

However, while the amplitude of the oscillations increase, so does the uncertainty for any miss distance estimate. For example with Orbit 1, after 2 days the average error could be calculated to be approximately 3 km. However, it could be 1.8 km or as bad as 5 km. After 4 days, the average error is just over 5 km with a minimum of 3 km and maximum approaching 9 km. Considering the suspected sources of this error growth, incorporating remaining higher order geopotential effects into the solution should pay dividends in increased solution accuracy over time.

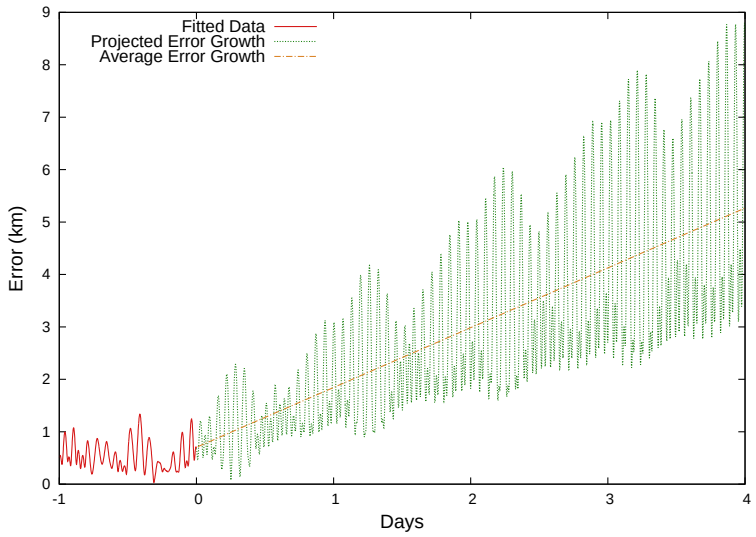

Figure 4.5: Magnitude of Error Growth: Orbit 1

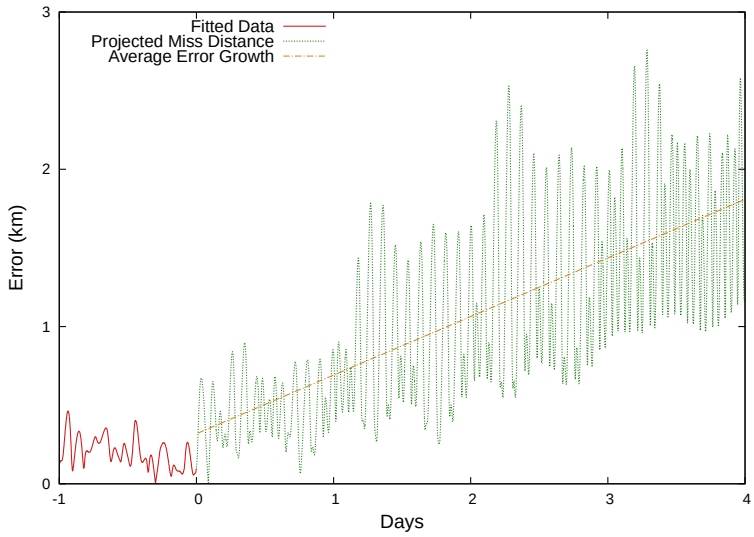

Figure 4.6: Magnitude of Error Growth: Orbit 2

4.3 Processing Time

A crucial attribute for general perturbations solutions such as Vinti is undoubtedly minimal overhead needed for computer processing. The goal of using Vinti in place of numerical integrators is similar accuracy with rapid processing. Also, as mentioned above, using numerical partials over analytical ones typically does not result in noticeable penalties. Although, in practice, this is not the case.

Wiesel's solution is still an analytical one in that it does not have to integrate the equations of motion for each time step along the way. It does, though, perform an integration to generate values needed for a specific orbit. Doing this once then propagating the state forward in time is still rapid. However, the fitting routine utilized for this research requires several orbital solutions to be calculated for each time step in order to create the numerical state transition for the purposes of fitting. This integration within Wiesel's solution is calculated dozens of times for each observation. This overhead makes it considerably slower than SGP4 but on the same order of time it takes to numerically

integrate a trajectory of similar duration. Performing orbit fitting using an analytical Phi matrix should alleviate this penalty.

4.4 Conclusion

Using only the solvable part of Vinti's solution as modified by Wiesel, this chapter fit orbits perturbed by the full geopotential. Performance, as compared to SGP4, is initially promising considering no attempts have been made to incorporate perturbations beyond the Vinti geopotential in an effort to close the gap towards the full geopotential. However, limitations were identified with high inclination and in terms of speed. Solutions near high inclination were not expected to produce poor results due to the original Vinti solution being advertised as free of singularities. Considering the popularity of such orbits in practice, this is a major drawback for operational application. With regards to speed, a rapid analytical solution was sought. However, using numerical partials for orbit fitting slows the process down enough where processing time for fits are about the same as integration. This provides motivation to repeat fitting development with aide of analytical partial matrices which is suggested for future works. The next chapter explores a method to add perturbations to the Vinti solution.

V. Air Drag

This chapter lays out an approach to account for and incorporate air drag effects in Vinti OD. The great advantage of possessing the closed form action-angle solution to the system will be exploited to perform classical perturbation theory. Being able to express the dynamics in such a unique way provides valuable and straightforward manipulation of coupling effects when adding perturbations.

An extensive review of the literature reveals this approach has not been applied to the original solution of Vinti or the modification due to Wiesel. The methodology is similar in theory to what Wiesel lays out in his text [35:202-205] and demonstrates in his analysis of periodic orbits with low eccentricity [73:3,10-19]. Small displacements to a multiply periodic system are considered and then a small perturbing acceleration is added. This forcing term is then Fourier-analyzed and integrated, providing a function of time for the perturbations. An analytical solution is then available to calculate displacements due to drag at any given time.

5.1 Air Drag Considered

Up until now, our dynamics have been assumed to be deterministic. This is to say that there is no random component involved, whether or not we can accurately account for it. However, there is one aspect of orbital motion that can be most likened to having random behavior and not included yet: air drag. Intuitively speaking, it does not seem important to consider the effects of air flowing over a spacecraft body. However, in space, air interacts by amassing several small collisions, one particle at a time, which is contrary to the idea of it "flowing." At such speeds, even the small mass of air molecules impart a significant perturbing acceleration over time through these tremendous collisions. Of course, this

effect diminishes as orbital altitudes increase and atmospheric density decreases. For low earth satellites, this is the dominant perturbation after the earth's geopotential.

Modern efforts have been made to develop somewhat deterministic models for the earth's atmosphere. This could provide information to the dynamics model in planning for and accurately quantifying the effect of air drag. However, the behavior of the atmosphere is exceedingly complex and dependent upon a number of phenomena that are effectively unpredictable. Needless to say, this aspect of our dynamics model contains the most amount of stochastic, or random, behavior. An adequate consideration of air drag is needed to make Vinti's solution relevant to modern OD.

Several techniques have been used through the years to include the dissipative effects of air drag in orbital motion solutions. The original SGP used a simplistic mean motion approximation while SGP4 uses power density functions [9]. In 1973, Vinti published a method to include perturbing forces in his original solution [43]. He proposed a set of Gaussian variational equations to solve for osculating elements in terms of the variables he used. This method examines changes to the separation coordinates and momenta, α_i and β_i. Although similar in principal, the current effort will work in actions and angles, $\mathcal{I}_i$ and θ_i. These variables are unique to Wiesel's modification of Vinti's solution and, thus, have not been examined previously as a means to solve for air drag.

5.2 Using Perturbation Theory

Demonstration of the underlying theory and solution derivation in this section will be displayed in the Cartesian reference frame. This is performed for clarity even though the system is solved through various changes of variables.

Recalling §3.1, we can express the equations of motion of the unperturbed Vinti system as

$$\dot{\mathbf{X}} = \mathbf{f}(\mathbf{X}, t) \tag{3.1}$$

or as an explicit solution

$$\mathbf{X}(t) = \mathbf{h}(\mathbf{X}(t_0), t). \tag{3.2}$$

where $\mathbf{X} = (x, y, z, \dot{x}, \dot{y}, \dot{z})^T$. These relations of a reference orbit are calculated by the Vinti solution as modified by Wiesel. Now, write Hamilton's equations as

$$\dot{\mathbf{X}} = \mathcal{Z}\frac{\partial \mathcal{H}}{\partial \mathbf{X}} \tag{5.1}$$

where

$$\mathcal{Z} = \begin{pmatrix} \emptyset & I \\ -I & \emptyset \end{pmatrix} \tag{5.2}$$

is the symplectic group matrix and preserves the properties

$$\mathcal{Z}^{-1} = \mathcal{Z}^T = -\mathcal{Z} \tag{5.3}$$

Now, linearize the Hamiltonian around the reference orbit and add a forcing, perturbing acceleration. We can now consider small changes to the reference system as

$$\delta\dot{\mathbf{X}} = \mathcal{Z}\frac{\partial^2 \mathcal{H}}{\partial \mathbf{X}^2}\delta\mathbf{X} + \dot{\mathbf{X}}_{\text{pert}} \tag{5.4}$$

Including this acceleration in the variational equation follows the general assumption in perturbation theory that the perturbation will remain small. In the case of air drag, this assumption only fails during the final stages of orbital decay when the flight profile is drastically altered by the exponentially growing atmospheric density. The drag perturbation can be inserted here and shown as

$$\dot{\mathbf{X}}_{\text{drag}} = \begin{pmatrix} \dot{\mathbf{r}}_{\text{drag}} \\ \dot{\mathbf{v}}_{\text{drag}} \end{pmatrix} = \begin{pmatrix} 0 \\ \mathbf{a}_{\text{drag}} \end{pmatrix} \tag{5.5}$$

where

$$\mathbf{a}_{\text{drag}} = -\frac{1}{2}\frac{C_d A \rho_{\text{ref}}}{m}\frac{\rho}{\rho_{\text{ref}}}|\mathbf{v}|\mathbf{v} \tag{5.6}$$

Combine the leading constant terms into a modified ballistic coefficient,

$$B^* = \frac{C_d A \rho_{\text{ref}}}{2m} \tag{5.7}$$

where C_d, A, and m are the satellite's drag coefficient, frontal area, and mass, respectively. Further, ρ_{ref} is the atmospheric density at perigee while ρ is the density at the satellite's location. (See §5.8 for details concerning the atmosphere model) The drag acceleration is now

$$\mathbf{a}_{\text{drag}} = -B^* \frac{\rho}{\rho_{\text{ref}}} |\mathbf{v}| \mathbf{v} \tag{5.8}$$

This expression for the drag acceleration can be found in Vallado[27:114] and Wiesel[73:3]. For special perturbations, this set of equations would be given to numerical integrators for solving; that, however, would defeat the purpose of the current research of seeking out a rapid analytical solution. However, certain numerical techniques can be utilized to exploit their benefit while employing an analytical method. The next section demonstrates this.

5.3 General Perturbations in Action-Angle Form

Consider a change of variables to action-angle form where $\mathbf{Y} = (\theta_1, \theta_2, \theta_3, \mathcal{I}_1, \mathcal{I}_2, \mathcal{I}_3)^T$ and $\mathcal{K}$ is the Hamiltonian in terms of these new variables, or more concisely,

$$\mathbf{Y} = \begin{pmatrix} \boldsymbol{\theta} \\ \boldsymbol{\mathcal{I}} \end{pmatrix} \tag{5.9}$$

and

$$\dot{\mathbf{Y}} = \begin{pmatrix} \dot{\boldsymbol{\theta}} \\ \dot{\boldsymbol{\mathcal{I}}} \end{pmatrix} = \mathcal{Z} \frac{\partial \mathcal{K}}{\partial \mathbf{Y}} = \begin{pmatrix} \boldsymbol{\omega} \\ 0 \end{pmatrix} \tag{5.10}$$

where the three frequencies, ω_i, correspond to the rate of change of each of Vinti's action-angles coordinates. As is consistent with the action-angle formulation, this says the angles, θ_i, increment linearly in time according to these basis frequencies while the conjugate momenta, $\mathcal{I}_i$, remain constant.

With this in mind, return to

$$\delta\dot{\mathbf{X}} = \mathcal{Z} \frac{\partial^2 \mathcal{H}}{\partial \mathbf{X}^2} \delta\mathbf{X} + \dot{\mathbf{X}}_{\text{pert}} \tag{5.4}$$

and change variables

$$\delta\dot{\mathbf{Y}}_{\text{total}} = \mathcal{Z}\frac{\partial^2\mathcal{K}}{\partial\mathbf{Y}^2}\delta\mathbf{Y} + \dot{\mathbf{Y}}_{\text{drag}} = A\delta\mathbf{Y} + \frac{\partial\mathbf{Y}}{\partial\mathbf{X}}\dot{\mathbf{X}}_{\text{drag}} \tag{5.11}$$

where

$$A = \begin{pmatrix} 0 & \frac{\partial\omega}{\partial\mathcal{I}} \\ 0 & 0 \end{pmatrix} \tag{5.12}$$

The Jacobian matrix relating small changes in the Cartesian frame to those in action-angle variables,

$$\frac{\partial\mathbf{X}}{\partial\mathbf{Y}} = \frac{\partial(\mathbf{r},\mathbf{v})}{\partial(\boldsymbol{\theta},\boldsymbol{\mathcal{I}})} \tag{5.13}$$

and the frequency partials matrix, $\frac{\partial\omega}{\partial\mathcal{I}}$, are calculated numerically within Wiesel's solution using a similar method to the one presented in §3.1.5.1 for finding the Phi matrix. Then, assuming this mapping between X and Y is one-to-one, continuous, and differentiable between 0 and 2π, the matrix $\frac{\partial\mathbf{X}}{\partial\mathbf{Y}}$ is inverted to change drag accelerations into action-angle form. The forcing term in Equation 5.11 then becomes

$$\dot{\mathbf{Y}}_{\text{drag}} = \begin{pmatrix} \delta\dot{\boldsymbol{\theta}} \\ \delta\dot{\boldsymbol{\mathcal{I}}} \end{pmatrix}_{\text{drag}} = \left[\frac{\partial(\mathbf{r},\mathbf{v})}{\partial(\boldsymbol{\theta},\boldsymbol{\mathcal{I}})}\right]^{-1}\begin{pmatrix} \dot{\mathbf{r}} \\ \dot{\mathbf{v}} \end{pmatrix}_{\text{drag}} = \begin{pmatrix} \frac{\partial\boldsymbol{\theta}}{\partial\mathbf{r}} & \frac{\partial\boldsymbol{\theta}}{\partial\mathbf{v}} \\ \frac{\partial\boldsymbol{\mathcal{I}}}{\partial\mathbf{r}} & \frac{\partial\boldsymbol{\mathcal{I}}}{\partial\mathbf{v}} \end{pmatrix}\begin{pmatrix} 0 \\ -B^*\frac{\rho}{\rho_{ref}}|\mathbf{v}|\mathbf{v} \end{pmatrix} \tag{5.14}$$

It follows that

$$\delta\dot{\boldsymbol{\theta}}_{\text{drag}} = \left(\frac{\partial\boldsymbol{\theta}}{\partial\mathbf{v}}\right)\mathbf{a}_{\text{drag}} \tag{5.15}$$

and

$$\delta\dot{\boldsymbol{\mathcal{I}}}_{\text{drag}} = \left(\frac{\partial\boldsymbol{\mathcal{I}}}{\partial\mathbf{v}}\right)\mathbf{a}_{\text{drag}} \tag{5.16}$$

We now have an expression for the change to the Vinti action-angle solution due to air drag. It is with this system of equations that an analytical solution will be sought.

5.4 Express as Fourier Series

The expected behavior of this forcing term will be assumed to be periodic or, at the least, contain periodic components. This is reasonable considering the local changes in

atmospheric density experienced by a satellite around a non-circular orbit. At perigee, the density is at a maximum and reduces to a minimum at apogee. This value oscillates between minimum and maximum as the satellite revolves at a period commensurate with that of the orbital period.

Since there is periodic behavior in this set of nonlinear, coupled equations, it should be easily expressed as multiple Fourier series that are functions of θ. To demonstrate finding the coefficients needed for this formulation, consider the changes per B^* due to drag (denoted by a prime),

$$\frac{\dot{\mathbf{Y}}_{\text{drag}}}{B^*} \equiv \dot{\mathbf{Y}}'_{\text{drag}} = \mathbf{f}(\boldsymbol{\theta}) \tag{5.17}$$

Changes to the system are considered on a *per* B^* basis for number conditioning reasons. Return to

$$\mathbf{a}_{\text{drag}} = -\frac{1}{2}\frac{C_d A \rho_{\text{ref}}}{m}\frac{\rho}{\rho_{\text{ref}}}|\mathbf{v}|\mathbf{v} \tag{5.6}$$

and considering

$$B^* = \frac{C_d A \rho_{\text{ref}}}{2m} \tag{5.7}$$

notice that the reference air density is combined into the leading B^* parameter and then divided out. Considering each term within

$$\mathbf{a}_{\text{drag}} = -B^*\frac{\rho}{\rho_{\text{ref}}}|\mathbf{v}|\mathbf{v} \tag{5.8}$$

the drag coefficient is very small ($B^* << 1$), yet constant. However, atmospheric density at the satellite's altitude divided by the reference density is near order unity. Likewise, the term $|\mathbf{v}|\mathbf{v}$ is of similar order because dimensionless, earth-based distance and time units result in a magnitude of velocity near 1 for most low earth orbits. Thus, it is numerically desirable to analyze and solve the function $\dot{\mathbf{Y}}_{\text{drag}}$ divided by B^*. After a solution is calculated for a certain size, shape, and orientation of orbit, this constant can then be multiplied back in for a specific satellite.

Looking at Equation 5.6 for the acceleration due to drag, it does not appear to contain a direct relation with the angle, θ_i. This functional dependence will be computed by incrementing the three angles from 0 to 2π in succession, calculating velocity and density values along the way resulting in acceleration quantities for each angle combination. Next, the following equations

$$\begin{aligned} \boldsymbol{C}_{\mathbf{j}} &= \left(\frac{1}{2\pi}\right)^3 \iiint_0^{2\pi} \mathbf{f}(\boldsymbol{\theta}) * \cos(\mathbf{j}\cdot\boldsymbol{\theta}) d\theta_1 d\theta_2 d\theta_3 \\ \boldsymbol{S}_{\mathbf{j}} &= \left(\frac{1}{2\pi}\right)^3 \iiint_0^{2\pi} \mathbf{f}(\boldsymbol{\theta}) * \sin(\mathbf{j}\cdot\boldsymbol{\theta}) d\theta_1 d\theta_2 d\theta_3 \end{aligned} \tag{5.18}$$

are solved using a rapid and straightforward Simpson's rule integration. An elaborate integration scheme is not necessary here due to the expected slow-changing behavior of the forcing term as a function of theta.

After the coefficients are in hand and following Wiesel's notation[35:191] (see next section), this series looks like

$$\begin{pmatrix} \delta\dot{\boldsymbol{\theta}}' \\ \delta\dot{\boldsymbol{I}}' \end{pmatrix}_{\text{drag}} = \begin{pmatrix} \frac{\partial\boldsymbol{\theta}}{\partial\mathbf{v}}\frac{\dot{\mathbf{v}}_{\text{drag}}}{B^*} \\ \frac{\partial\boldsymbol{I}}{\partial\mathbf{v}}\frac{\dot{\mathbf{v}}_{\text{drag}}}{B^*} \end{pmatrix} = \boldsymbol{C}_0 + \sum_{\mathbf{j}\neq 0}\left[\boldsymbol{C}_{\mathbf{j}} cos\,(\mathbf{j}\cdot\omega t) + \boldsymbol{S}_{\mathbf{j}} sin\,(\mathbf{j}\cdot\omega t)\right] \tag{5.19}$$

This representation is a set of six Fourier series where $\boldsymbol{C}_{\mathbf{j}}$, $\boldsymbol{S}_{\mathbf{j}}$ are vector coefficients with $\mathbf{j}$ being a vector summation index[11]. The dot products $\mathbf{j}\cdot\boldsymbol{\omega}$ are linear combinations of the basis frequencies. These frequencies multiplied by time give the angle coordinates.

In this form, finding a solution to these equations is straightforward. Analytically integrate Equation 5.19 with respect to time to result in the system of equations

$$\begin{pmatrix} \delta\boldsymbol{\theta}' \\ \delta\boldsymbol{I}' \end{pmatrix}_{\text{drag}} = \boldsymbol{C}_0(t-t_0) + \sum_{\mathbf{j}\neq 0}\left[\frac{\boldsymbol{C}_{\mathbf{j}}}{\mathbf{j}\cdot\boldsymbol{\omega}} sin\,(\mathbf{j}\cdot\omega t) - \frac{\boldsymbol{S}_{\mathbf{j}}}{\mathbf{j}\cdot\boldsymbol{\omega}} cos\,(\mathbf{j}\cdot\omega t)\right]\Bigg|_{t_0}^{t} \tag{5.20}$$

[11] Due to sine/cosine ambiguities ($\sin -x = -\sin x$, etc.), the first non-zero index shall not be negative

Moving forward, it will be necessary to make some abbreviations for brevity. Return to Equation 5.19 and these key elements of the Fourier series may be expressed as

$$\begin{pmatrix} \delta\dot{\boldsymbol{\theta}}' \\ \delta\dot{\boldsymbol{I}}' \end{pmatrix} = \begin{pmatrix} \boldsymbol{C}_0^{\boldsymbol{\theta}} + \mathcal{F}\mathcal{S}_{\dot{\boldsymbol{\theta}}} \\ \boldsymbol{C}_0^{\boldsymbol{I}} + \mathcal{F}\mathcal{S}_{\dot{\boldsymbol{I}}} \end{pmatrix} \tag{5.21}$$

with the corresponding solution being

$$\begin{pmatrix} \delta\boldsymbol{\theta}' \\ \delta\boldsymbol{I}' \end{pmatrix} = \begin{pmatrix} \boldsymbol{C}_0^{\boldsymbol{\theta}}(t - t_0) + \mathcal{F}\mathcal{S}_{\boldsymbol{\theta}} \\ \boldsymbol{C}_0^{\boldsymbol{I}}(t - t_0) + \mathcal{F}\mathcal{S}_{\boldsymbol{I}} \end{pmatrix} \tag{5.22}$$

The lead, constant coefficient will use the same notation because it does not change when integrated.

This section showed how the forcing, drag accelerations can be expressed and manipulated. Including these changes in the global solution requires an extra, deliberate step, to be presented in §5.6.

5.5 An Example Using Vector Indices

An example of using summation indices in this fashion will now be offered to provide clarity. Consider one of the six equations to be expressed with this method. For instance, changes to θ_1 due to drag could resemble a multiply periodic relation such as

$$\dot{\theta}_1 = 2.4 - 4.1\sin(-\theta_2 + \theta_3) + 0.3\cos(\theta_1 - 2\theta_2) + 1.7\cos(\theta_1 - \theta_3) \tag{5.23}$$

Table 5.1 illustrates how these would be stored. Since $\theta_i = \omega_i t$, the integrated solution with respect to time becomes

$$\theta_1 = 2.4t + \frac{4.1}{-\omega_2 + \omega_3}\cos(-\theta_2 + \theta_3) + \frac{0.3}{\omega_1 - 2\omega_2}\sin(\theta_1 - 2\theta_2) + \frac{1.7}{\omega_1 - \omega_3}\sin(\theta_1 - \theta_3) \tag{5.24}$$

Table 5.2 shows how these solution indices would be stored. These indices can now be summed whenever a solution at a specific time is desired using the summation convention presented earlier.

Table 5.1: Expressing Summation Quantities

j_1	j_2	j_3	$C_{\mathbf{j}}$	$S_{\mathbf{j}}$
0	0	0	2.4	-
0	-1	1	0	-4.1
1	-2	0	0.3	0
1	0	-1	1.7	0

Table 5.2: Expressing Solution Summation Quantities

j_1	j_2	j_3	$C_{\mathbf{j}}$	$S_{\mathbf{j}}$
0	0	0	2.4	-
0	-1	1	$\frac{4.1}{-\omega_2+\omega_3}$	0
1	-2	0	0	$\frac{0.3}{\omega_1-2\omega_2}$
1	0	-1	0	$\frac{1.7}{\omega_1-\omega_3}$

5.6 Small Changes to a Coupled System

Now that the forcing term is expressed by a multiple Fourier series, changes to the system as a whole can be considered. Return to

$$\delta\dot{\mathbf{Y}}_{\text{total}} = \mathcal{Z}\frac{\partial^2\mathcal{K}}{\partial\mathbf{Y}^2}\delta\mathbf{Y} + \dot{\mathbf{Y}}_{\text{drag}} = A\delta\mathbf{Y} + \frac{\partial\mathbf{Y}}{\partial\mathbf{X}}\dot{\mathbf{X}}_{\text{drag}} \tag{5.11}$$

and rewrite

$$\begin{pmatrix} \delta\dot{\boldsymbol{\theta}}' \\ \delta\dot{\boldsymbol{\mathcal{I}}}' \end{pmatrix}_{\text{total}} = \begin{pmatrix} 0 & \frac{\partial\omega}{\partial\mathcal{I}} \\ 0 & 0 \end{pmatrix}\begin{pmatrix} \delta\boldsymbol{\theta}' \\ \delta\boldsymbol{\mathcal{I}}' \end{pmatrix} + \dot{\mathbf{Y}}'_{\text{drag}} \tag{5.25}$$

leaving

$$\begin{aligned} \delta\dot{\boldsymbol{\theta}}'_{\text{total}} &= \frac{\partial\boldsymbol{\omega}}{\partial\boldsymbol{\mathcal{I}}'}\delta\boldsymbol{\mathcal{I}}' + \delta\dot{\boldsymbol{\theta}}'_{\text{drag}} \\ \delta\dot{\boldsymbol{\mathcal{I}}}'_{\text{total}} &= 0 + \delta\dot{\boldsymbol{\mathcal{I}}}'_{\text{drag}} \end{aligned} \tag{5.26}$$

Notice that the angle equations are coupled with those of momenta. Luckily, the latter can be solved directly because the only change in momenta is due to drag.

Return to the Fourier solution

$$\begin{pmatrix} \delta\boldsymbol{\theta}' \\ \delta\boldsymbol{\mathcal{I}}' \end{pmatrix}_{\text{drag}} = \boldsymbol{C}_0(t-t_0) + \sum_{\mathbf{j}\neq 0}\left[\frac{\boldsymbol{C}_{\mathbf{j}}}{\mathbf{j}\cdot\boldsymbol{\omega}}sin\left(\mathbf{j}\cdot\boldsymbol{\omega}t\right) - \frac{\boldsymbol{\mathcal{S}}_{\mathbf{j}}}{\mathbf{j}\cdot\boldsymbol{\omega}}cos\left(\mathbf{j}\cdot\boldsymbol{\omega}t\right)\right]\Bigg|_{t_0}^{t} \tag{5.20}$$

and only consider the momenta series. Using abbreviations introduced in §5.4, this solution can be expressed as

$$\delta\boldsymbol{\mathcal{I}}'_{\text{total}} = \delta\boldsymbol{\mathcal{I}}'_{\text{drag}} = \boldsymbol{C}_0^{\mathcal{I}}(t-t_0) + \mathcal{F}\mathcal{S}_{\mathcal{I}}\Big|_{t_0}^{t} = \boldsymbol{C}_0^{\mathcal{I}}t + \mathcal{F}\mathcal{S}_{\mathcal{I}}(t) - \delta\boldsymbol{\mathcal{I}}'_{drag}(t_0). \tag{5.27}$$

where $\delta\boldsymbol{\mathcal{I}}'_{drag}(t_0)$ combines constant and periodic contributions to momenta at the initial time. Then, inserting this into the total angles solution, Equation 5.26 becomes

$$\delta\dot{\boldsymbol{\theta}}'_{\text{total}} = \frac{\partial\boldsymbol{\omega}}{\partial\boldsymbol{\mathcal{I}}}\left(\boldsymbol{C}_0^{\mathcal{I}}t + \mathcal{F}\mathcal{S}_{\mathcal{I}}(t) - \delta\boldsymbol{\mathcal{I}}'(t_0)\right) + \boldsymbol{C}_0^{\theta} + \mathcal{F}\mathcal{S}_{\dot{\theta}} \tag{5.28}$$

Separate constant from periodic terms and integrate this with respect to time, leaving

$$\delta\boldsymbol{\theta}'_{\text{total}} = \frac{\partial\boldsymbol{\omega}}{\partial\boldsymbol{\mathcal{I}}}\left(\frac{1}{2}\boldsymbol{C}_0^{\mathcal{I}}(t^2-t_0^2) - \delta\boldsymbol{\mathcal{I}}'(t_0)(t-t_0)\right) + \boldsymbol{C}_0^{\theta}(t-t_0) + \int_{t_0}^{t}\left(\frac{\partial\boldsymbol{\omega}}{\partial\boldsymbol{\mathcal{I}}}\mathcal{F}\mathcal{S}_{\mathcal{I}}(t) + \mathcal{F}\mathcal{S}_{\dot{\theta}}\right)dt \tag{5.29}$$

This shows that a linear drift in the momenta from the lead, constant coefficient becomes quadratic in the angle.

Now, combine like coefficients while expanding the periodic portions

$$\begin{aligned}\delta\boldsymbol{\theta}'_{\text{total}} = {} & \frac{\partial\boldsymbol{\omega}}{\partial\boldsymbol{\mathcal{I}}}\left(\frac{1}{2}\boldsymbol{C}_0^{\mathcal{I}}(t^2-t_0^2) + \delta\boldsymbol{\mathcal{I}}'(t_0)(t-t_0)\right) + \boldsymbol{C}_0^{\theta}(t-t_0) \\ & + \int_{t_0}^{t}\sum_{\mathbf{j}\neq 0}\left\{\left[\boldsymbol{C}_{\mathbf{j}}^{\theta} - \frac{\partial\boldsymbol{\omega}}{\partial\boldsymbol{\mathcal{I}}}\frac{\boldsymbol{\mathcal{S}}_{\mathbf{j}}^{\mathcal{I}}}{\mathbf{j}\cdot\boldsymbol{\omega}}\right]cos\left(\mathbf{j}\cdot\boldsymbol{\omega}t\right) + \left[\boldsymbol{\mathcal{S}}_{\mathbf{j}}^{\theta} + \frac{\partial\boldsymbol{\omega}}{\partial\boldsymbol{\mathcal{I}}}\frac{\boldsymbol{C}_{\mathbf{j}}^{\mathcal{I}}}{\mathbf{j}\cdot\boldsymbol{\omega}}\right]sin\left(\mathbf{j}\cdot\boldsymbol{\omega}t\right)\right\}dt\end{aligned} \tag{5.30}$$

then integrate the periodic portion

$$\begin{aligned}\delta\boldsymbol{\theta}'_{\text{total}} = {} & \frac{\partial\boldsymbol{\omega}}{\partial\boldsymbol{\mathcal{I}}}\left(\frac{1}{2}\boldsymbol{C}_0^{\mathcal{I}}(t^2-t_0^2) + \delta\boldsymbol{\mathcal{I}}'(t_0)(t-t_0)\right) + \boldsymbol{C}_0^{\theta}(t-t_0) \\ & + \sum_{\mathbf{j}\neq 0}\left\{\left[\frac{\boldsymbol{C}_{\mathbf{j}}^{\theta}}{\mathbf{j}\cdot\boldsymbol{\omega}} - \frac{\partial\boldsymbol{\omega}}{\partial\boldsymbol{\mathcal{I}}}\frac{\boldsymbol{\mathcal{S}}_{\mathbf{j}}^{\mathcal{I}}}{(\mathbf{j}\cdot\boldsymbol{\omega})^2}\right]sin\left(\mathbf{j}\cdot\boldsymbol{\omega}t\right) - \left[\frac{\boldsymbol{\mathcal{S}}_{\mathbf{j}}^{\theta}}{\mathbf{j}\cdot\boldsymbol{\omega}} + \frac{\partial\boldsymbol{\omega}}{\partial\boldsymbol{\mathcal{I}}}\frac{\boldsymbol{C}_{\mathbf{j}}^{\mathcal{I}}}{(\mathbf{j}\cdot\boldsymbol{\omega})^2}\right]cos\left(\mathbf{j}\cdot\boldsymbol{\omega}t\right)\right\}\Bigg|_{t_0}^{t}\end{aligned} \tag{5.31}$$

Equations 5.27 and 5.31 complete incorporating small changes due to air drag into perturbations of the global solution. These small changes can then be converted back to Cartesian space and added to the predicted state as provided by the Vinti solution at a given time. This conversion is performed using previously supplied matrix, $\frac{\partial \mathbf{X}}{\partial \mathbf{Y}}$ from Equation 5.13. Incorporating these changes into orbit fitting as explained in Chapter III will be discussed in §5.9.

5.7 Possible Resonances

In practice, for all orbits attempted, the three basis frequencies returned by the Vinti solution were very nearly equal each other. The difference between any two are on the order of 10^{-3}. Considering the summation indices that account for all the linear combinations of frequencies, there are certain combinations that could be problematic.

For instance, the frequency combination that corresponds to the index $(1, 0, -1)$ would mean ω_3 would be subtracted from ω_1 resulting in a very small number. Looking at the momentum solution in Equation 5.20, this number is in the denominator of the new coefficients. In the original frequency analysis, if any of the coefficients are non-negligible this new term will become noticeable. This effect is then exacerbated when the momenta solution is then integrated again to provide the angle solution. See how this term is then squared in Equation 5.31. Now, a term that was merely noticeable before is now significant. This indicates that there is a possibility for resonances when accounting for drag using this method.

As an example, consider Orbit 2. Table 5.3 shows a couple sets of coefficients found for the first of the six equations. Anything smaller than 10^{-8} is approximated as zero. It is important to note that the majority of the coefficient pairs are zero for the various angle combinations.

Table 5.3: Example Coefficients For Orbit 2, Coordinate 1

j_1	j_2	j_3	$C_\mathbf{j}$	$S_\mathbf{j}$
1	2	0	0	1.64e-2
2	-2	0	0	2.01e-2

Considering the resulting basis frequencies for this orbit are $\boldsymbol{\omega}^T = (0.85042, 0.85126, 0.85047)$, Table 5.4 shows the new coefficients after analytical integration of the equations. Notice how for the first angle combination, the absolute value of the coefficient decreased by more than half as a result of dividing by $\omega_1 + 2\omega_2$ or $(0.85042 + 2 * 0.85126)$. However, for the second combination, it is divided by $2\omega_1 - 2\omega_2$ or $2*(0.85042 - 0.85126) = -0.00168$. This increases the value of the coefficient by four orders of magnitude from 2.01e-2 to -5.86e+2.

Table 5.4: Example Integrated Coefficients For Orbit 2, Coordinate 1

j_1	j_2	j_3	$C_\mathbf{j}$	$S_\mathbf{j}$
1	2	0	-6.90e-3	0
2	-2	0	-5.86e+2	0

5.8 Atmosphere Model

This investigation uses an atmosphere model developed by Regan and Anandakrishnan. Instead of a purely exponential model for density as a function of reference density and height, it breaks the atmosphere into different layers of strata. Using a hybrid methodology, it uses the US 1976 Standard Atmosphere for altitudes from 0 to 86 km and the US 1962 Standard Atmosphere model for altitudes above 86 km. This older model for higher

altitudes simplifies calculations greatly by using linear lapse rates instead of exponential and elliptical ones found in two of the higher strata levels. These minor differences have been argued by Regan and Anandakrishnan to pale in comparison to other changes in atmospheric density that are less predictable, e.g. incoming solar radiation. Being consistent with the motivation of the current research, this approach was chosen to maintain simplistic, rapid computer processing while demonstrating a relatively accurate solution method. [78]

In reality, the altitude used to determine this density profile pertains to height above the geoid. Constant lines of density actually take on the shape of earth, which is not spherical. Therefore, extra calculations are needed to determine local altitude relative to the ground at any given time. The current research will, however, only use spherical altitude. Obviously, there may exist slight differences in exact densities by neglecting nonspherical effects. However, the truth model and perturbation routine will both make this assumption. This commonality can still provide a validation of the method presented.

5.9 Incorporating Drag Into Orbit Fitting

Recall from Chapter III how the Phi matrix is calculated at each observation then used for orbit fitting. Changes to the six state variables at some epoch time are related to those at an observation time through the $6x6$ state transition matrix. This is then used in the accumulated equation

$$\delta\mathbf{X}(t_0) = (T^T Q^{-1}\ T)^{-1}\ T^T Q^{-1}\ \mathbf{r} \tag{5.32}$$

which solves for six corrections to the state variables using only three residuals (remember $T = H\Phi$ from Equation 3.7). This mechanism allows for a convenient avenue by which to calculate and store the necessary quantities needed to adjust the Vinti orbit as affected by drag.

Add a seventh state to solve for B^*. Now, the modified state vector is $\mathbf{X}' = (x, y, z, \dot{x}, \dot{y}, \dot{z}, B^*)^T$ and $\dot{B}^* = 0$. Perform partials of the state at time t with respect to

the state at t_0 to get the modified Phi matrix

$$\mathbf{\Phi}'(t,t_0) = \left[\begin{array}{cccc|c} \frac{\partial x(t)}{\partial x(t_0)} & \frac{\partial x(t)}{\partial y(t_0)} & \cdots & \frac{\partial x(t)}{\partial \dot{z}(t_0)} & \frac{\partial x(t)}{\partial B^*} \\ \frac{\partial y(t)}{\partial x(t_0)} & \frac{\partial y(t)}{\partial y(t_0)} & \cdots & \frac{\partial y(t)}{\partial \dot{z}(t_0)} & \frac{\partial y(t)}{\partial B^*} \\ \vdots & \vdots & \ddots & \vdots & \vdots \\ \frac{\partial \dot{z}(t)}{\partial x(t_0)} & \frac{\partial \dot{z}(t)}{\partial y(t_0)} & \cdots & \frac{\partial \dot{z}(t)}{\partial \dot{z}(t_0)} & \frac{\partial \dot{z}(t)}{\partial B^*} \\ \hline 0 & 0 & \ldots & 0 & 1 \end{array}\right] \tag{5.33}$$

The bottom row is 0 because the drag coefficient is considered a constant. Notice the new values in the last column. These are changes in the X state with respect to B^*. However, the formulations in previous sections solved for changes to the action-angle variables per B^*. Arriving at these X-space quantities requires using the previously found partials matrix (see Equation 5.13) to perform a change of variables from theta and momenta to position and velocity.

The additional fitting process to incorporate drag for a given observation follows. Before the fitting routine kicks off, perform the Fourier analysis discussed earlier to calculate coefficients for the six series as in Equation 5.18. These involve constant and periodic coefficients. Return to Equation 5.20 and solve each of the six equations at a given time with the drag coefficient divided out. This solution is rapid considering only time needs to be supplied for multiplication then summing over the Fourier series. These values provide incremental quantities of the action-angle variables per B^*. Convert these values to Cartesian space by

$$\frac{\partial\left(\mathbf{r},\mathbf{v}\right)(t)}{\partial B^*} = \frac{\partial\left(\mathbf{r},\mathbf{v}\right)}{\partial\left(\boldsymbol{\theta},\boldsymbol{\mathcal{I}}\right)} \frac{\delta\left(\boldsymbol{\theta},\boldsymbol{\mathcal{I}}\right)(t)}{B^*} \tag{5.34}$$

and save them in the Phi matrix.

In parallel, the original Phi parameters are determined normally. The fitting scheme then continues for each iteration as described earlier until convergence is declared. B^* is now a "solve for" parameter giving the routine another setting to adjust in hopes of an optimal orbit solution. This is reasonable considering the difficulty involved in determining

a craft's B^* value at a specific time. This value is in theory a constant but realistically as the satellite changes orientation, the frontal area relative to its direction of travel can vary. Further, accurately determining a vehicle's drag coefficient (C_D) poses difficult without a wind tunnel that can replicate orbital velocities and densities.

5.10 Results

Test orbit 1 (parameters can be found in Table 3.1) is analyzed using this procedure. This orbit is low in the atmosphere and should provide a baseline with which to demonstrate capability. This approach calculates changes in theta and momenta per B^* so results should be able to scaled for various realistic drag parameters.

Recall that the development of the variational action-angle relations in §5.6 revealed the angle solution is dependent upon, or coupled with, that of the momenta. So looking at momenta perturbations first, Figure 5.1 shows the total change due to drag over one day. Notice the varied effects across the three momenta. Momenta 1 is near constant while momenta 2 and 3 change linearly. The change in momentum 3 is more pronounced and also exhibits a periodic oscillation of seemingly constant amplitude. Through the coupling matrix $\frac{\partial \omega}{\partial I}$, this noticeable change in momenta affects all three angles. As predicted in Equation 5.31, Figure 5.2 shows that this linear growth manifests as a quadratic θ drift. The first angle experiences a periodic affect but all three have near equal secular quadratic growth. Note that the behavior of angles 2 and 3 in the figure are identical.

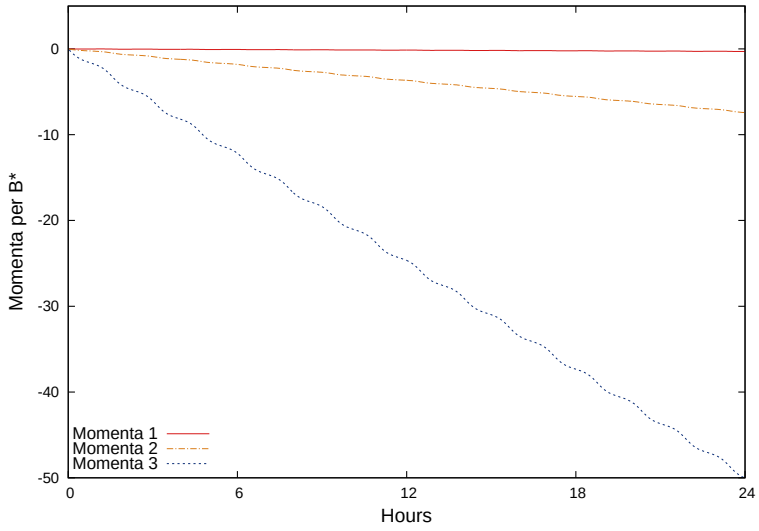

Figure 5.1: Momenta Perturbations

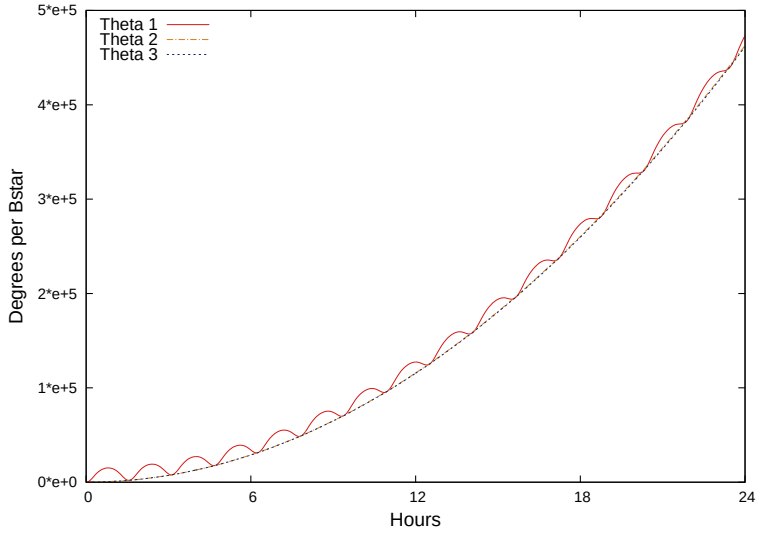

Figure 5.2: Theta Perturbations

To approximate model error, a fourth-order Hamming numerical integration algorithm accounting for air drag will serve as a truth model. It is modified slightly to call upon the Vinti solution package in order to output action-angles periodically. The geopotential of this model has also been adjusted to mimic that of Vinti's. Therefore, the only perturbations

compared with this model are those due to drag. Since the integrated trajectory is perturbed by the same atmosphere model, these instantaneous values represent osculating Vinti parameters and can then be compared to the analytically predicted values at commensurate time steps.

Figures 5.3 and 5.4 show the differences in momenta and angle between the current approach and the integrated truth model. These differences are presented as percentage errors of the calculated truth. Momenta 2 and 3 exhibit a linear increase in percentage error and equal about 3.5% after one day. It is interesting to note that the expected quantity of momentum 3 is about 5 times greater than momenta 2 but the percent error is identical in magnitude and behavior with the exception of the initial transient. It is important to note that erratic behavior displayed in some errors near $t = 0$ are a result of a small divisor in calculating percent error. The difference in perturbations is divided by the magnitude of integrated pertubation which is 0 at the initial time and very small for the first few timesteps. Figure 5.5 shows error growth for a more extended time. The predicted angle perturbations are approximately 87% correct after 5 days.

5.11 Conclusions

Consistent with the motivations of the current research, numerical integration of the equations of motion has been avoided. What resulted is a straightforward formulation of how air drag should affect the reference orbit. This solution allows for a relation to be determined ahead of orbit fitting that results in a function of time. Linear changes in momenta resulted in quadratic angle as expected. The angle solution from techniques presented in this chapter remain 97.5% and 87% correct after 1 and 5 days, respectively.

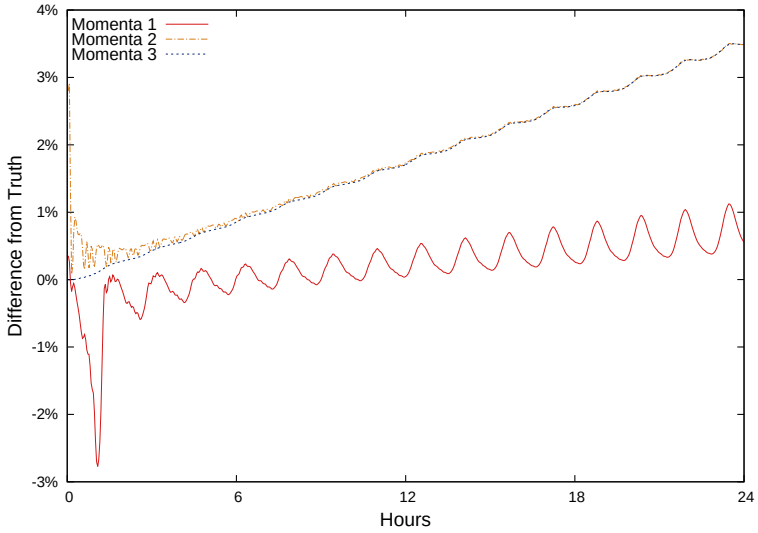

Figure 5.3: Error in Momenta Perturbations

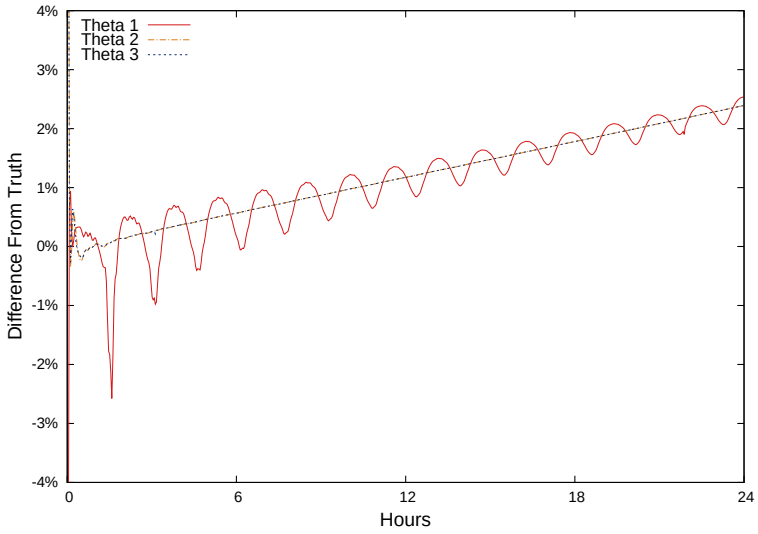

Figure 5.4: Error in Angle Perturbations

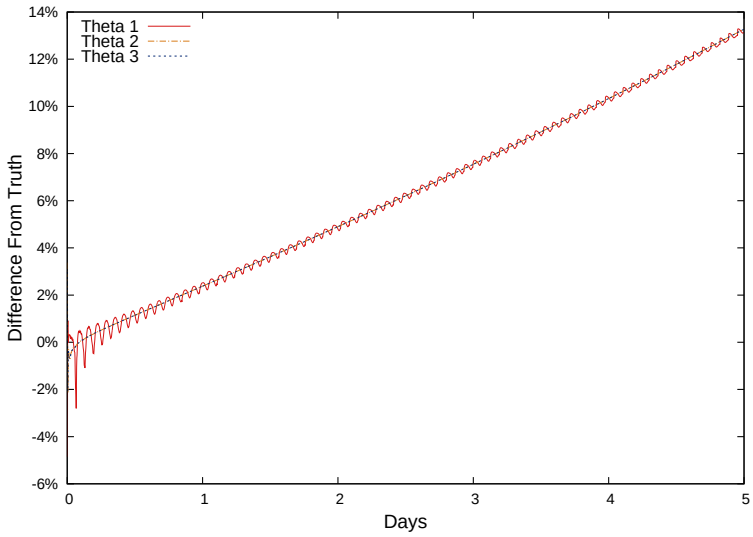

Figure 5.5: Error in Angle Perturbations Over 5 Days

VI. Air Drag - An Alternate Approach

The author's motivation for implementing the type of perturbation technique presented in Chapter V was having the action-angle variables available to generate an integrable analytical function. As a validation of this technique using the Vinti solution, an alternate approach is presented and results are compared. This chapter will implement a similar formulation using another dynamical system with actions and angles.

6.1 General Perturbations Using Two Body Action-Angles

As discussed earlier in §2.7, obtaining these unique action-angle quantities for the two body problem using the Hamilton-Jacobi theory results in Delauney variables. Although the two body problem is fully degenerate, the one available frequency (due to the mean anomaly) is the most relevant to air drag perturbations since the dissipating effect is mostly in-track or in the velocity direction. It is intuitive to imagine the satellite would slow down in its orbital plane due to air drag more than the node would be shifted for an inclined orbit.

Using two body problem variables with equations of motion

$$\dot{\mathbf{X}}_{TBP} = \mathbf{f}(\mathbf{X}, t) = \begin{pmatrix} \mathbf{v} \\ -\mu\mathbf{r}/r^3 \end{pmatrix} \tag{6.1}$$

consider air drag perturbations as a forced linear system. Linearize around a reference orbit and add a small forcing term to obtain the equations for small changes to the system. Similar to before, this can be expressed as

$$\delta\dot{\mathbf{X}} = A(t)\delta\mathbf{X} + \dot{\mathbf{X}}_{drag} \tag{6.2}$$

where $A(t) = \nabla\mathbf{f}$ and

$$A(t) \approx \left[\begin{array}{c|c} \emptyset & I \\ \hline A_{2,1} & \emptyset \end{array}\right] \tag{3.21}$$

For the two body problem, the gravity acceleration terms found in the lower left sub-matrix are

$$A_{2,1} = \begin{bmatrix} -\frac{\mu}{r^3} + \frac{3\mu x^2}{r^5} & \frac{3\mu xy}{r^5} & \frac{3\mu xz}{r^5} \\ \frac{3\mu xy}{r^5} & -\frac{\mu}{r^3} + \frac{3\mu y^2}{r^5} & \frac{3\mu yz}{r^5} \\ \frac{3\mu xz}{r^5} & \frac{3\mu yz}{r^5} & -\frac{\mu}{r^3} + \frac{3\mu z^2}{r^5} \end{bmatrix} \tag{6.3}$$

Another way to express the variational changes of the physical variables is by relating them to Delauney elements through a matrix of partial derivatives. This conveys as

$$\delta\mathbf{X} = \frac{\partial\mathbf{X}}{\partial\mathbf{D}}\delta\mathbf{D} \tag{6.4}$$

Remember from before that these elements are $\mathbf{D} = (L, G, H, l, g, h)$ where L, G, H are constant momenta and l, g, h are corresponding angles and are related to the orbital elements as

$$\begin{aligned} L &= \sqrt{\mu a} & l &= M \\ G &= L\sqrt{1-e^2} & g &= \omega \\ H &= G\cos i & h &= \Omega \end{aligned} \tag{2.1}$$

For the two body problem, all values are constant except the mean anomaly, M, which varies according to mean motion, $n = \sqrt{\frac{\mu}{a^3}}$. Now, take a time derivative of Equation 6.4,

$$\delta\dot{\mathbf{X}} = \left(\frac{d}{dt}\frac{\partial\mathbf{X}}{\partial\mathbf{D}}\right)\delta\mathbf{D} + \frac{\partial\mathbf{X}}{\partial\mathbf{D}}\delta\dot{\mathbf{D}} \tag{6.5}$$

Possessing two ways to express the same quantity, set Equation 6.2 equal to Equation 6.5, substitute for $\delta\mathbf{X}$,

$$\frac{d}{dt}\frac{\partial\mathbf{X}}{\partial\mathbf{D}}\delta\mathbf{D} + \frac{\partial\mathbf{X}}{\partial\mathbf{D}}\delta\dot{\mathbf{D}} = A(t)\frac{\partial\mathbf{X}}{\partial\mathbf{D}}\delta\mathbf{D} + \dot{\mathbf{X}}_{drag} \tag{6.6}$$

and solve for the element rate of change,

$$\delta\dot{\mathbf{D}} = \left(\frac{\partial\mathbf{X}}{\partial\mathbf{D}}\right)^{-1}\left\{A(t)\delta\mathbf{X} - \frac{d}{dt}\frac{\partial\mathbf{X}}{\partial\mathbf{D}}\right\}\delta\mathbf{D} + \left(\frac{\partial\mathbf{X}}{\partial\mathbf{D}}\right)^{-1}\dot{\mathbf{X}}_{drag} \tag{6.7}$$

again assuming that the mapping between Cartesian and Delauney variables is one-to-one, continuous, and differentiable from 0 to 2π. Similar to before with Vinti, we now have an expression for the change to the TBP action-angle solution due to air drag with which we can seek an analytical solution.

6.2 Another Coupled System

At first glance, this expression for the time rate of change of small changes to Delauney elements as perturbed by air drag does not seem to have the same coupling effect on the lead term as the expression found for similar changes to Vinti action-angles. From Chapter V, the expression for total variations for Vinti

$$\delta\dot{\mathbf{Y}}_{\text{total}} = \mathcal{Z}\frac{\partial^2\mathcal{K}}{\partial\mathbf{Y}^2}\delta\mathbf{Y} + \dot{\mathbf{Y}}_{\text{drag}} = A\delta\mathbf{Y} + \frac{\partial\mathbf{Y}}{\partial\mathbf{X}}\dot{\mathbf{X}}_{\text{drag}} \tag{5.11}$$

shows the solution is multiplied by A which is

$$A = \begin{pmatrix} 0 & \frac{\partial\omega}{\partial I} \\ 0 & 0 \end{pmatrix} \tag{5.12}$$

and constant. This alternate approach arriving at the expression for TBP elements contains the matrices $\frac{\partial\mathbf{X}}{\partial\mathbf{D}}$ and A_{TBP} which are actually periodic in this application. However, when subtracted to form the entire leading term that multiplies $\delta\mathbf{D}$ it becomes a constant matrix like before in the Vinti relation. However, only one element is non-negligible as can be seen in a representative output of this matrix:

$$\begin{bmatrix} 2.27\text{e-}013 & 5.68\text{e-}014 & 8.53\text{e-}014 & -2.65\text{e+}000 & -1.63\text{e-}009 & 9.95\text{e-}014 \\ -1.99\text{e-}013 & -8.53\text{e-}014 & -2.84\text{e-}014 & -1.75\text{e-}009 & 1.86\text{e-}009 & 7.11\text{e-}015 \\ -1.39\text{e-}017 & 5.55\text{e-}017 & -1.10\text{e-}016 & 2.10\text{e-}013 & -1.14\text{e-}013 & -4.44\text{e-}016 \\ 1.33\text{e-}015 & 1.11\text{e-}015 & 8.88\text{e-}016 & -2.84\text{e-}014 & 1.14\text{e-}013 & -2.78\text{e-}017 \\ 1.33\text{e-}015 & 8.88\text{e-}016 & 8.88\text{e-}016 & 2.84\text{e-}014 & 1.42\text{e-}013 & -2.78\text{e-}017 \\ 8.88\text{e-}016 & 4.44\text{e-}016 & 8.88\text{e-}016 & -5.68\text{e-}014 & 1.14\text{e-}013 & 1.11\text{e-}016 \end{bmatrix}$$

This turns out to be element $[1, 4]$ which couples the solution of the first action momenta into changes in the first angle, the mean anomaly. This is unlike before in Equation 5.12 where the upper right block of the matrix was non-zero which coupled all the momenta solutions back into all angle variations. So, all small variations to action and angles for

Delauney are equal only to the effect due to drag with the exception of the mean anomaly and this is coupled with the corresponding momenta. This becomes

$$\begin{aligned} \delta\dot{\theta}_1 &= c\mathcal{I}_1 + \delta\dot{\theta}_{1,drag} \\ \delta\dot{\theta}_{i\neq 1} &= \delta\dot{\theta}_{i\neq 1,drag} \end{aligned} \tag{6.8}$$

and

$$\delta\dot{\boldsymbol{\mathcal{I}}}_{\text{total}} = \delta\dot{\boldsymbol{\mathcal{I}}}_{\text{drag}} \tag{6.9}$$

Return to Equation 6.7 and compare the forcing term to the one found before in Equation 5.11. The mechanics of the air drag perturbation are the same but differs in the relation between Cartesian and action-angle coordinates. We are now ready to analyze these expressions and calculate a solution using the technique presented previously.

6.3 Fourier Series Approach Revisited

Possessing the forcing relation between Cartesian and Delauney variables due to air drag as well as the coupling effect between mean anomaly and its momenta, analysis will follow the steps prescribed in §5.4. Using the same atmosphere model and take the new forcing term

$$\frac{\dot{\mathbf{D}}_{\text{drag}}}{B^*} \equiv \dot{\mathbf{D}}'_{\text{drag}} = \mathbf{f}(\boldsymbol{\theta}) \tag{6.10}$$

and express it as a Fourier Series

$$\begin{pmatrix} \delta\dot{\boldsymbol{\theta}}' \\ \delta\dot{\boldsymbol{\mathcal{I}}}' \end{pmatrix}_{\text{drag}} = \begin{pmatrix} \frac{\partial\boldsymbol{\theta}}{\partial\mathbf{v}}\frac{\dot{\mathbf{v}}_{\text{drag}}}{B^*} \\ \frac{\partial\boldsymbol{\mathcal{I}}}{\partial\mathbf{v}}\frac{\dot{\mathbf{v}}_{\text{drag}}}{B^*} \end{pmatrix} = \boldsymbol{C}_0 + \sum_{\mathbf{j}\neq 0}\left[\boldsymbol{C}_{\mathbf{j}} cos\left(\mathbf{j}\cdot\boldsymbol{\omega}t\right) + \boldsymbol{\mathcal{S}}_{\mathbf{j}} sin\left(\mathbf{j}\cdot\boldsymbol{\omega}t\right)\right] \tag{5.19}$$

Solving as before this becomes

$$\begin{pmatrix} \delta\boldsymbol{\theta}' \\ \delta\boldsymbol{\mathcal{I}}' \end{pmatrix}_{\text{drag}} = \boldsymbol{C}_0(t-t_0) + \sum_{\mathbf{j}\neq 0}\left[\frac{\boldsymbol{C}_{\mathbf{j}}}{\mathbf{j}\cdot\boldsymbol{\omega}} sin\left(\mathbf{j}\cdot\boldsymbol{\omega}t\right) - \frac{\boldsymbol{\mathcal{S}}_{\mathbf{j}}}{\mathbf{j}\cdot\boldsymbol{\omega}} cos\left(\mathbf{j}\cdot\boldsymbol{\omega}t\right)\right]\Bigg|_{t_0}^{t} \tag{5.20}$$

Since five of the terms are not coupled, this is their direct solution for changes due to air drag. In the case of mean anomaly, the coupling term needs to be considered. With the

momenta solution inserted and recalling the notation presented in §5.4, the angle time rate of change is

$$\delta\dot{\theta}'_{1,\text{total}} = c_1 \left(C_0^{\mathcal{I}_1} t + \mathcal{FS}_{\mathcal{I}_1}(t) - \delta\mathcal{I}'_1(t_0) \right) + C_0^{\theta_1} + \mathcal{FS}_{\dot{\theta}_1} \tag{6.11}$$

Integrating this analytically, the solution becomes

$$\begin{aligned} \delta\theta'_{1,\text{total}} = {} & c_1 \left(\frac{1}{2} C_0^{\mathcal{I}_1} t^2 + \delta\mathcal{I}'_1(t_0)(t - t_0) \right) + C_0^{\theta_1}(t - t_0) \\ & + \sum_{\mathbf{j}\neq 0} \left\{ \left[\frac{C_{\mathbf{j}}^{\theta_1}}{\mathbf{j}\cdot\boldsymbol{\omega}} - c_1 \frac{\mathcal{S}_{\mathbf{j}}^{\mathcal{I}_1}}{(\mathbf{j}\cdot\boldsymbol{\omega})^2} \right] sin\left(\mathbf{j}\cdot\boldsymbol{\omega}t\right) - \left[\frac{\mathcal{S}_{\mathbf{j}}^{\theta_1}}{\mathbf{j}\cdot\boldsymbol{\omega}} + c_1 \frac{C_{\mathbf{j}}^{\mathcal{I}_1}}{(\mathbf{j}\cdot\boldsymbol{\omega})^2} \right] cos\left(\mathbf{j}\cdot\boldsymbol{\omega}t\right) \right\} \Bigg|_{t_0}^{t} \end{aligned} \tag{6.12}$$

after expanding periodic terms and combining like terms.

Equations 5.20 and 6.12 complete the solutions for small changes to a TBP system under the influence of air drag only. We now possess a method to calculate perturbed Delauney actions and angles to compare with those from Vinti.

6.4 TBP Results

For the sake of comparison, test orbit 1 will be analyzed again using the current method. Identical orbits examined through two different lenses provide a basis to draw some conclusions on performance and behavior. Examining momenta first, Figure 6.1 shows momenta perturbations after one day.

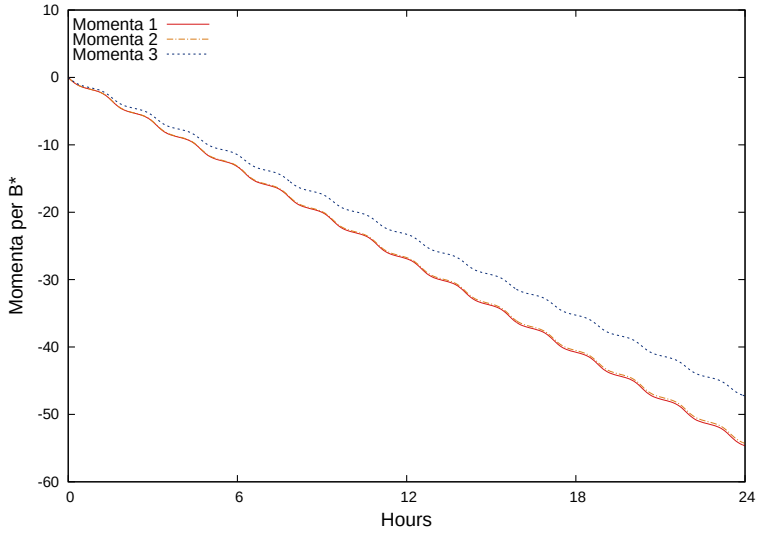

Figure 6.1: TBP Momenta Perturbations

Comparing Figure 5.1 to 6.1, the noticeable difference from what was presented for Vinti is how all momenta are affected now. Earlier, only the third momenta incremented linear in time and the rest were nearly constant. Remembering the expressions in Equation 2.1 for the TBP momenta this makes sense. Each quantity is directly proportionate to the semi-major axis, a. The first momenta, L, is $\sqrt{\mu a}$. The second momenta is multiplied by L, and the third momenta is multiplied by the second. Therefore, as the dissipative effect of air drag reduces the orbits energy and ultimately altitude, each momenta decreases accordingly. The rate of decrease will differ as functions of eccentricity or inclination. Otherwise, the magnitude of the effect is very similar. Differences from truth will be presented shortly then compared.

Now consider changes to the angle. Before with Vinti, each angle experienced quadratic effects due to the coupling effect with the one linear momenta perturbation. Figure 6.2 shows the results for TBP angles. As expected, the dominant effect manifests itself in the mean anomaly or parallel to the direction of travel. Again, the angle exhibits a quadratic shift with a periodic behavior consistent with the orbital frequency. The node and

argument of perigee are mainly constant with a slight periodic oscillation with the orbital frequency.

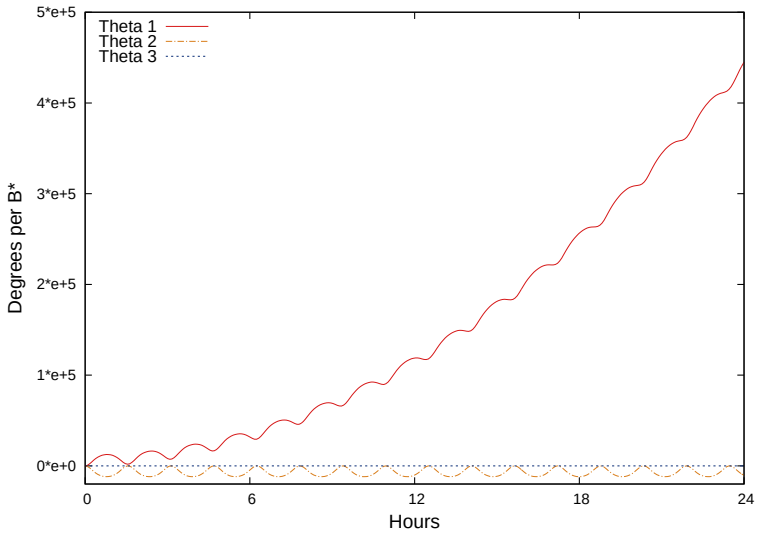

Figure 6.2: TBP Angle Perturbations

Using the same truth model as before but altered to output TBP quantities, results are compared. Figures 6.3 and 6.4 show the error in the current method as a percentage of the total calculated truth perturbation. The error growth compared to the total value of expected perturbations seems stable. The percentage growth of the momenta is linear and is on the order of 3% after one day.

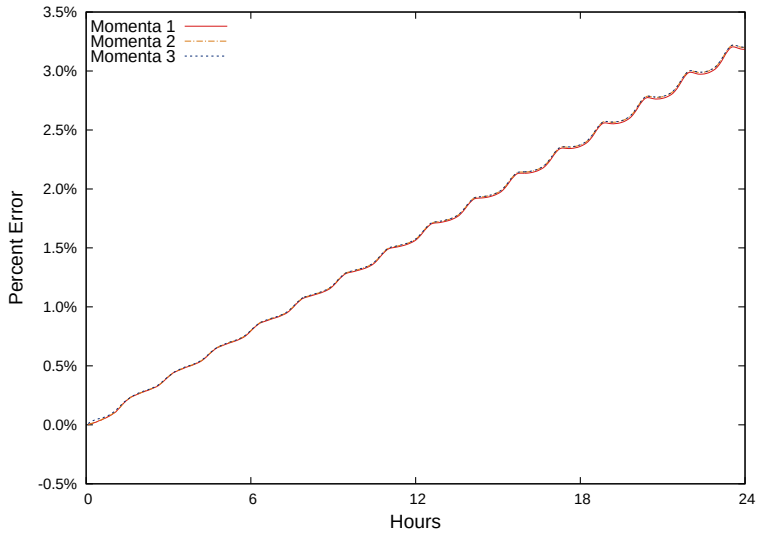

Figure 6.3: TBP Momenta Error

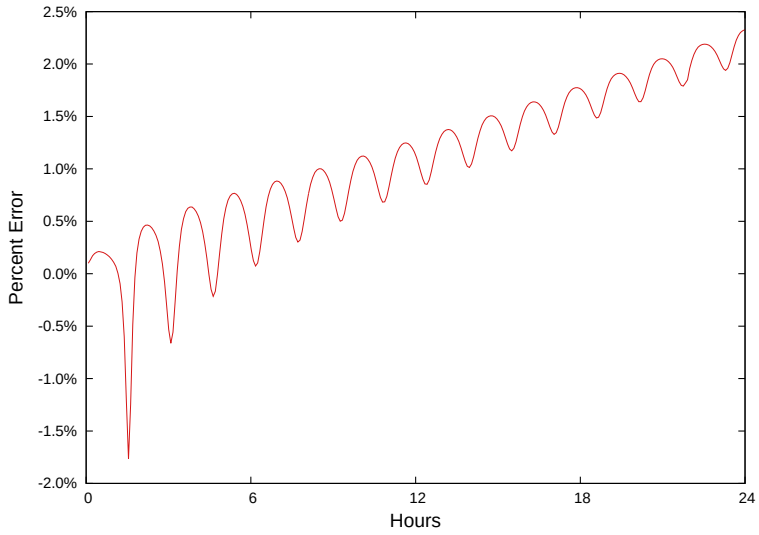

Figure 6.4: Mean Anomaly Error

As with the momenta (Figure 6.3), the mean anomaly percent error growth (Figure 6.4) appears linear. However, a more noticeable periodic behavior is present again corresponding with the orbital frequency. Figure 6.5 extends this prediction out five days

for perspective. The data suggest that this perturbation method remains about 98% accurate after one day and 88% accurate after five days with seemingly stable behavior. With this method, comparing error growth in the second and third angles is not necessary since there is no secular growth. Further, calculating a percent error is not feasible since it would require dividing by zero when the truth perturbation vanishes periodically.

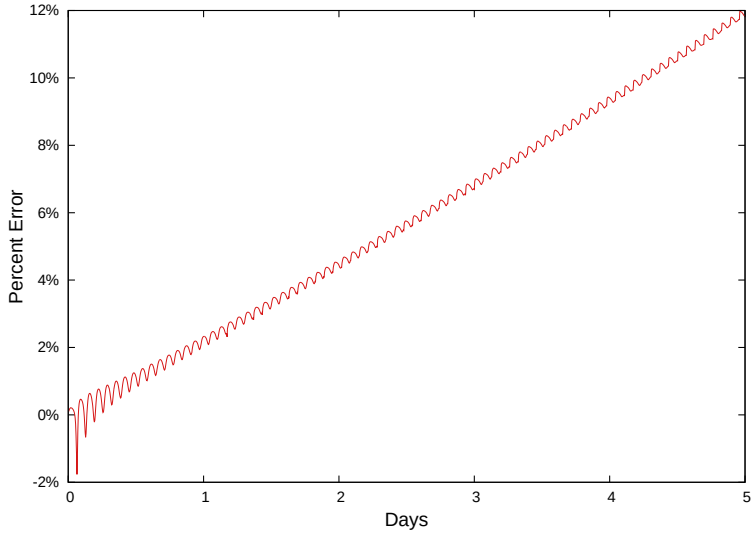

Figure 6.5: Mean Anomaly Error Over 5 Days

6.5 Conclusion

Although behavior is expectedly different in general, the magnitude of total perturbations expected and resulting errors are strikingly similar. This provides evidence that this analytical approach consisting of Fourier analysis and rapid solution calculation is valid. Furthermore, the twofold validation to demonstrate viability proves the newly modified Vinti solution is well suited for such an approach.

VII. Conclusion

7.1 Summary

A preliminary examination into the claimed "other solvable solution" has been presented. This solution is viewed as a candidate for a more comprehensive orbit determination tool with which to increase accuracy for space situational awareness purposes. In Chapters III and IV, a nonlinear least squares routine was developed then utilized to demonstrate the effectiveness of Vinti's modified solution for orbit fitting. Chapter V illustrated a novel approach for performing classical perturbations on this new solution using air drag. Chapter VI validated this approach by repeating the steps on a well known and understood system with similar and relevant characteristics.

Although it is not ready to be inserted into a workstation at JSPOC, Vinti's solution as modified by Wiesel holds great promise. Between the literature review into SGP4 accuracy and the comparisons made within this research, it is safe to say that orbit fitting using this solution returns very similar results to what is gained by the Air Force's analytical propagator. Of course, this is only true for a limited orbital regime.

7.2 Recommendations

Future work related to Wiesel's solution has a bright future although there are near-term limitations and obstacles to overcome. The potential capability and utility greatly outweighs these initial difficulties. A summary of efforts required to tap into these benefits follows.

- The current research developed and utilized a numerically calculated state transition matrix. This was accomplished due to the ease of implementation so research could begin with analyzing Wiesel's solution in a timely fashion. In theory, there should be minor trade-offs in performance due to computing time needed to simply go ahead

and calculate the values at each time step. In practice however, there is a significant different between using SGP4 for least squares fitting (which uses an analytically derived Phi matrix) and Vinti. An analytical Phi matrix for Vinti's solution should be explored and used for orbit fitting.

- Performance degradation experienced for solutions near polar orbit should be addressed. This inclination range is popular for various reasons. In order for this solution to be widely used and accepted for LEO, the inclination limitation needs removing. It is the author's belief the troubles lie in Wiesel's numerical integrals adversely affected by the negative argument of perigee rate between critical inclinations.

- The current research has only used the solvable solution approximating the behavior induced by the full geopotential. However, a perturbations approach to incorporate more of these effects is necessary. Including higher order geopotential perturbations should minimize periodic and secular growth in future error. This would result in accurate predictions being valid for an extended period of time.

- The next largest contributor to secular error growth over time for low earth satellites is air drag. Although a method accounting for air drag and a notional fitting technique was presented, orbit fitting using them was not demonstrated. This should be explored and could possibly be undertaken in parallel with either of the suggestions above.

- Accomplishing the three previous efforts would round out an effective and accurate orbit fitting scheme for LEO objects. Research should then move to incorporating other perturbing effects necessary for higher altitude orbits. These include luni-solar third body effects initially. Having developed a method to account for the sun and moon should translate easily to adding other desired bodies if necessary. Also, the air

drag scheme should prove adaptable to allowing for solar wind/radiation effects. The Fourier series sampling approach would only need to sample a different perturbing acceleration expression.

- Another, more advanced aspect of orbit determination could be examined that is unique to the small percentage of orbiting objects that are active, maneuverable satellites. The ability to identify and model a maneuver within a batch of observations would significantly increase utility for using Vinti in orbit fitting. Otherwise, these batches of observations would lend to poor results until an separate program sifted through the observations then provided Vinti with a new epoch state at the time of maneuver. That would only increase the dependence on other systems.

- When all the efforts are complete, a well-rounded and capable solution should be at hand. At that point, a more realistic and operationally relevant process should be examined. Computing efficiencies throughout the code could be implemented to keep processing time to a minimum. Also, observation relations for representative SSN data are required. Then, actual satellite data could be fit for true system performance.

7.3 A Parting Thought

With the exponential increase in objects orbiting earth, interest in inexpensive orbit determination coupled with accurate conjunction assessment will continue to rise. This will remain a top priority not only for the scientific community but also for international leadership. Considering the threat to US satellites by orbital debris, USAF General Lynn III said "Without space systems, many of our most important military advantages evaporate" [79]. This impetus should motivate the community to not allow analytical theory to stagnate and sit backseat to that of numerical. However, the marriage of analytical (using Vinti's solution) and numerical (using Wiesel's modification followed by Fourier expansions)

methods as described here has the potential to meet the need of the space monitoring community.

Appendix A: Vinti's Hamiltonian

Using Vinti's coordinate system, the conjugate momenta can be found as

$$\begin{aligned} p_\rho &= \frac{\rho^2 + c^2\eta^2}{c^2 + \rho^2}\dot{\rho} \\ p_\eta &= \frac{\rho^2 + c^2\eta^2}{1 - \eta^2}\dot{\eta} \\ p_\phi &= (1 - \eta^2)(c^2 + \rho^2)\dot{\phi} \end{aligned} \tag{A.1}$$

and using his potential

$$V = -\mu\frac{\rho + \eta\delta}{\rho^2 + c^2\eta^2} \tag{A.2}$$

the resulting Hamiltonian is

$$\mathcal{H} = \frac{1}{2}\left\{\frac{c^2 + \rho^2}{\rho^2 + c^2\eta^2}p_\rho^2 + \frac{1 - \eta^2}{\rho^2 + c^2\eta^2}p_\eta^2 + \frac{1}{(1 - \eta^2)(c^2 + \rho^2)}p_\phi^2\right\} - \frac{\mu\rho}{\rho^2 + c^2\eta^2} \tag{A.3}$$

Appendix B: Extra Figures

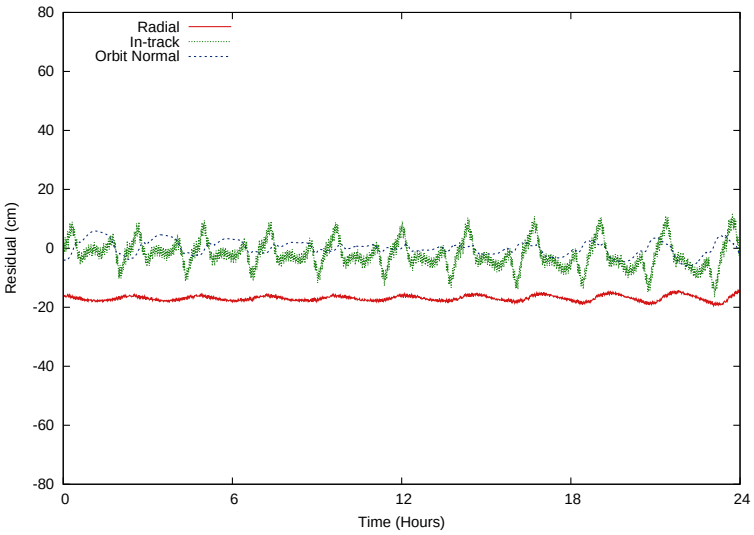

Figure B.1: Vinti Geopotential Fit Residuals: Orbit 3

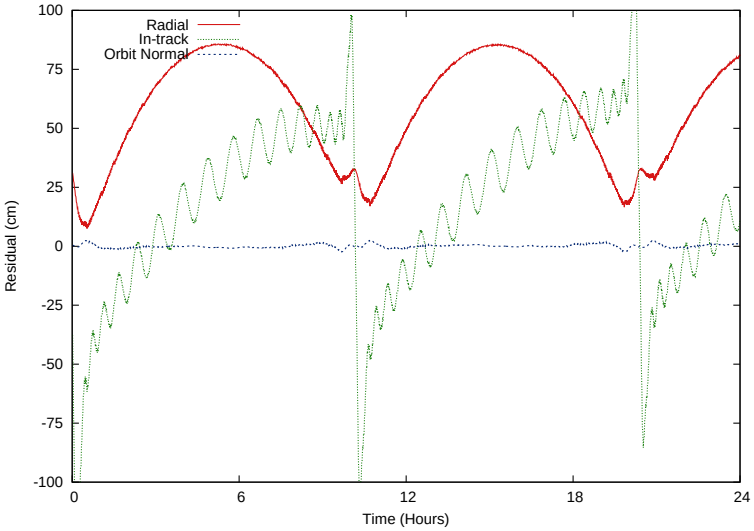

Figure B.2: Vinti Geopotential Fit Residuals: Orbit 4

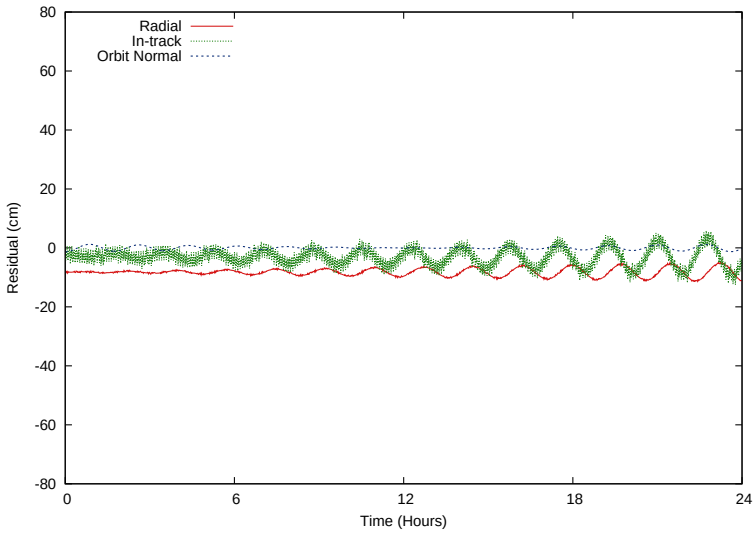

Figure B.3: Vinti Geopotential Fit Residuals: Orbit 5

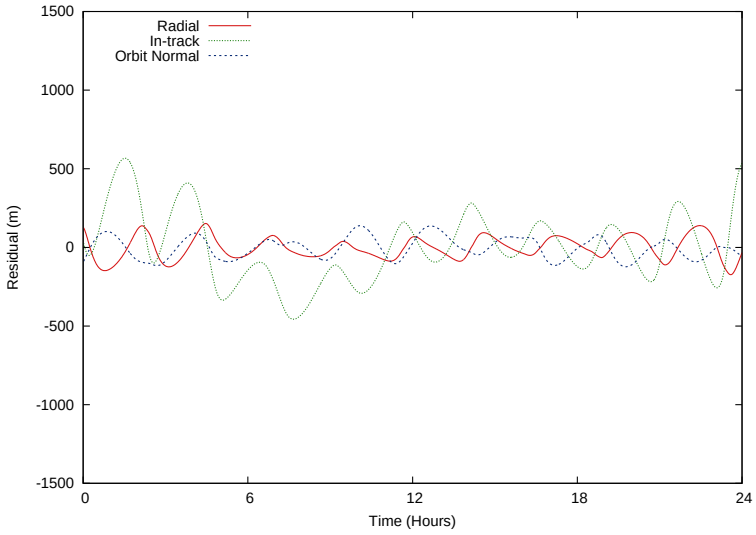

Figure B.4: Full Geopotential Fit Residuals: Orbit 3

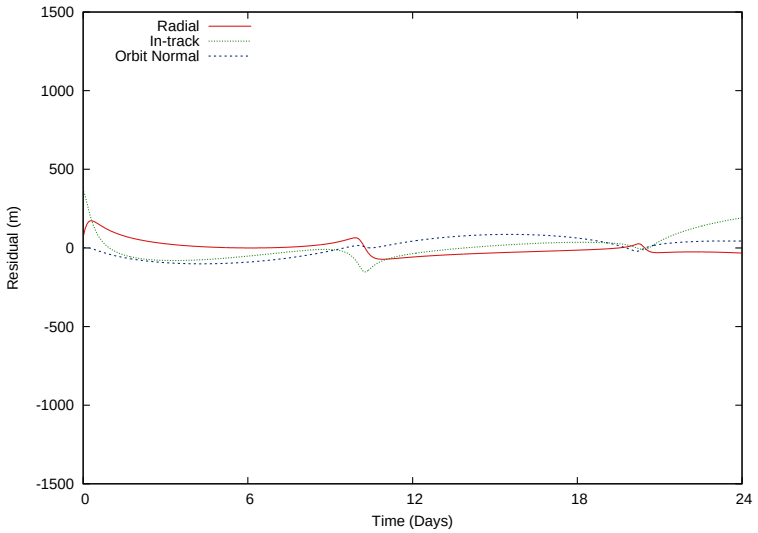

Figure B.5: Full Geopotential Fit Residuals: Orbit 4

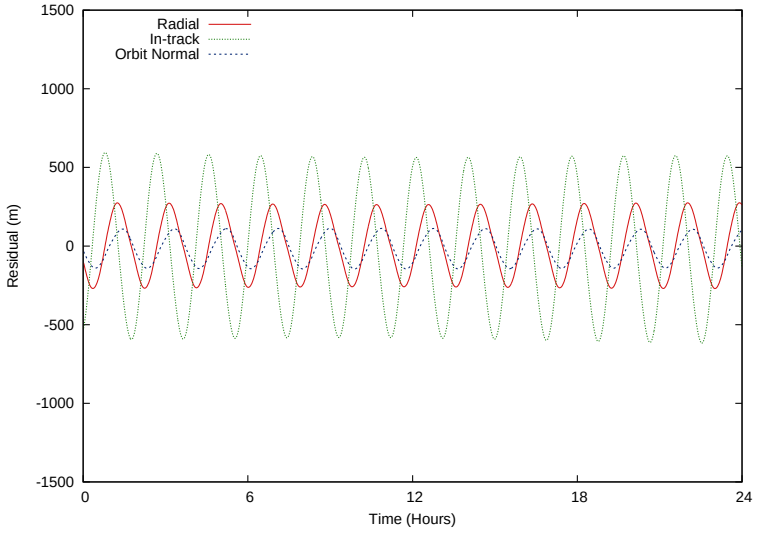

Figure B.6: Full Geopotential Fit Residuals: Orbit 5

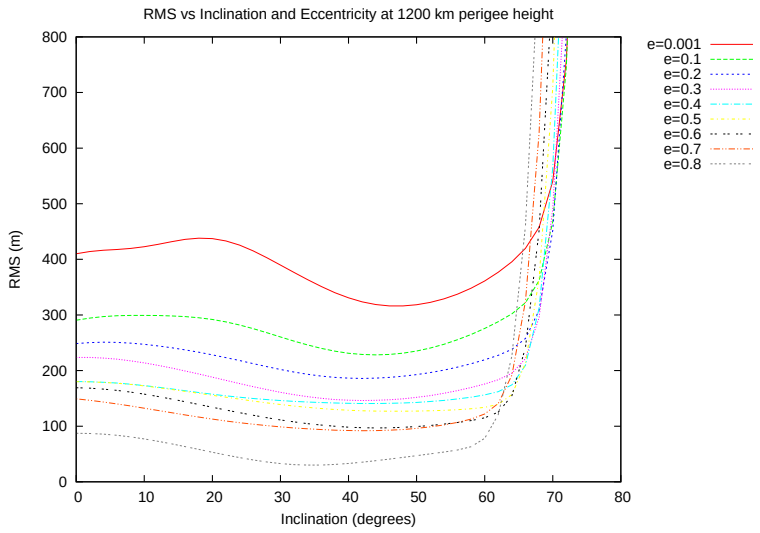

Figure B.7: Orbit Fit Performance: Perigee Height = 1200 km

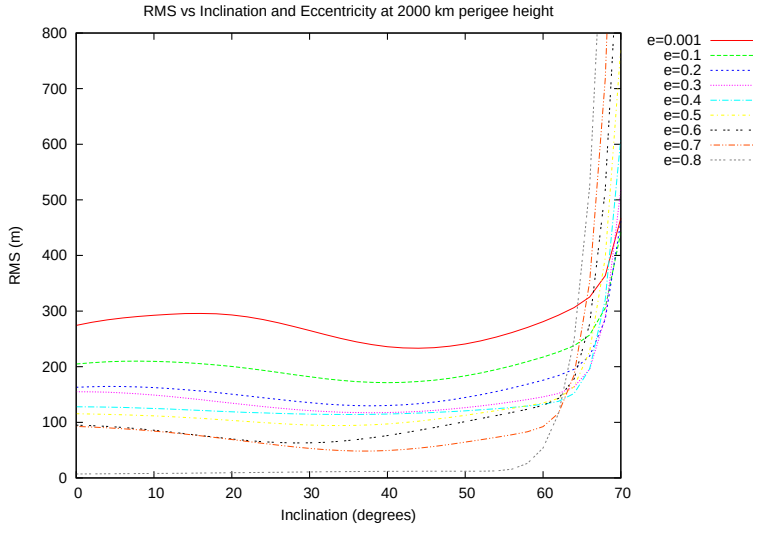

Figure B.8: Orbit Fit Performance: Perigee Height = 2000 km

Appendix C: The Critical Inclination

Under the influence of J_2 the expression for the secular effect on the argument of perigee is

$$\dot{\omega} = -\frac{3nJ_2Re^2}{2a^2(1-e^2)^2}\left(\frac{5}{2}\sin^2 i - 2\right) \tag{C.1}$$

and setting this rate equal to zero becomes

$$\frac{5}{2}\sin^2 i - 2 = 0 \tag{C.2}$$

which means this occurs at inclinations

$$i_c = \sin^{-1}\left(\frac{2}{\sqrt{5}}\right) \tag{C.3}$$

or angles of 63.4349^o and 116.5650^o. These are termed the critical inclination where the argument of perigee is fixed and the orbit does not rotate in its own plane. Below and above these inclinations, the orbit advances or the rate is positive. Between the two inclinations and straddling polar orbits, the argument of perigee backs up or the rate is negative. Figure C.1 qualitatively illustrates this.

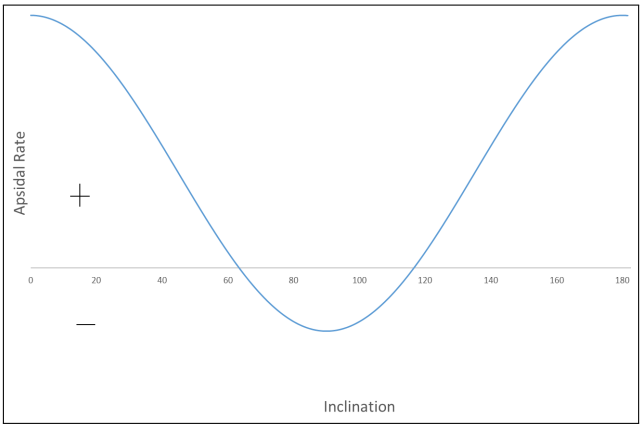

Figure C.1: J_2 Effect on Apsidal Rate

Bibliography

[1] Wright, D., "Colliding Satellites: Consequences and Implications," 2009, http://www.ucucsusa.org/assets/documents/nwgs/SatelliteCollision- 2-12-09.pdf.

[2] Chilton, K. P., "2009 Strategic Space Symposium - Commander's Perspective," 3 November 2009, http://www.stratcom.mil/speeches/2009/26/2009_Strategic_Space_Symposium_-_Commanders_Perspective/.

[3] Shelton, W. L., "Threats from Space: A Review of U.S. Government Efforts to Track and Mitigate Asteroids and Meteroids," *Department of the Air Force Presentation to the House Science, Space, and Technology Committee, U.S. House of Representatives*, 19 March 2013.

[4] https://www.space-track.org.

[5] Kelso, T. S., "Iridium 33/Cosmos 2251 Collision," July 2009, http://celestrak.com/events/collision.asp.

[6] Kelso, T. S., "Analysis of the Iridium 33-Cosmos 2251 Collision," *Maui: Advanced Maui Optical and Space Surveillance Technologies Conference*, 2009.

[7] Kehler, C. R., "29th National Space Symposium," 16 April 2013, http://www.stratcom.mil/speeches/2013/91/29th_National_Space_Symposium/.

[8] National Research Council, *Continuing Kepler's Quest: Assessing Air Force Space Command's Astrodynamics Standards*, National Academies Press, 2012.

[9] Vallado, D. A., Crawford, P., Hujsak, R., and Kelso, T. S., "Revisiting Spacetrack Report #3," *AIAA/AAS Astrodynamics Specialist Conference, 21-24 August 2006, Keystone, CO*.

[10] Vetter, J. R., "Fifty Years of Orbit Determination: Development of Modern Astrodynamics Methods," *Johns Hopkins APL Technical Digest*, Vol. 27, 2007, pp. 239–252.

[11] Levit, C. and Marshall, W., "Improved Orbit Predictions Using TLE Data," *Advances in Space Research*, Vol. 47, No. 7, April 2011, pp. 1107–1115.

[12] Greene, M. R. and Zee, R. E., "Increasing the Accuracy of Orbital Position Information from NORAD SGP4 Using Intermittent GPS Readings," *23rd Annual AIAA/USU Conference on Small Satellites*, 2009.

[13] Dong, W. and Chang-yin, Z., "An Accuracy Analysis of the SGP4/SDP4 Model," *Chinese Astronomy and Astrophysics*, Vol. 34, 2010, pp. 69–76.

[14] Hildreth, S. A. and Arnold, A., *Threats to U.S. National Security Interests in Space: Orbital Debris Mitigation and Removal*, Washington, D.C.: Congressional Research Service, January 8, 2014.

[15] Hyde, J., Christiansen, E., and Lear, D., "Orion EFT-1 Postflight MMOD Inspection," *Orbital Debris Quarterly News*, Vol. 19, April 2015, pp. 6–9.

[16] European Space Agency, "Space Surveillance and Tracking - SST Segment," http://www.esa.int/Our_Activities/Operations/Space_Situational_Awareness/Space_Surveillance_and_Tracking_-_SST_Segment.

[17] Liou, J. C. and Johnson, N. L., "Instability of the Present LEO Satellite Populations," *Advances in Space Research*, Vol. 41, 2008, pp. 1046–1053.

[18] Kessler, D. J. and Cour-Palais, B. G., "Collision Frequency of Artificial Satellites: The Creation of a Debris Belt," *Journal of Geophysical Research*, Vol. 83, No. A6, 1978, pp. 2637–2646.

[19] Tate, K., "Russian Satellite Crash with Chinese ASAT Debris Explained (Infographic)," March 03, 2013, http://www.space.com/20145-russian-satellite-chinese-debris-crash-infographic.html.

[20] Baiocchi D. and Welser IV, W., *Confronting Space Debris*, RAND Corporation, 2010.

[21] Vinti, J. P., "New Method of Solution for Unretarded Satellite Orbits," *Journal of Research of the National Bureau of Standards*, Vol. 62B, 1959, pp. 105–116.

[22] Vinti, J. P., *Orbital and Celestial Mechanics*, Vol. 177 of *Progress in Astronautics and Aeronautics*, American Institute of Aeronautics and Astronautics, 1801 Alexander Bell Dr. Restn, VA 20191, 1998.

[23] Wiesel, W. E., "Numerical Solution to Vinti's Problem," *Journal of Guidance, Control, and Dynamics*, Vol. 38, 2015, pp. 1757–1764.

[24] Hoots, J. F. R., Schumacher, P. W., and Glover, R. A., "A History of Analytical Orbit Modeling in the United States Space Surveillance System," *Journal of Guidance, Control, and Dynamics*, Vol. 27, 2004, pp. 174–185.

[25] Brouwer, D., "Solution of the Problem of Artificial Satellite Theory Without Drag," *The Astronomical Journal*, Vol. 64, No. 1274, 1959, pp. 378–396.

[26] Kozai, Y., "The Motion of a Close Earth Satellite," *The Astronomical Journal*, Vol. 64, 1959, pp. 367–377.

[27] Vallado, D. A., *Fundamentals of Astrodynamics and Applications*, Microcosm Press and Kluwer Academic Publishers, 3rd ed., 2007.

[28] Kozai, Y., "Second-Order Solution of Artificial Satellite Theory Without Air Drag," *The Astronomical Journal*, Vol. 67, 1962, pp. 446–461.

[29] Garfinkel, B., "The Orbit of a Satellite of an Oblate Planet," *The Astronomical Journal*, Vol. 64, No. 1274, 1959, pp. 353–366.

[30] Lyddane, R. H., "Small Eccentricities or Inclinations in the Brouwer Theory of the Artificial Satellite," *The Astronomical Journal*, Vol. 68, No. 8, 1963, pp. 555–558.

[31] Deprit, A., "Canonical Transformations Depending on a Small Parameter," *Celestial Mechanics*, Vol. 1, 1969, pp. 12–30.

[32] Brouwer, D. and Hori, G., "Theoretical Evaluation of Atmospheric Drag Effects in the Motion of an Artificial Satellite," *Astronomical Journal*, Vol. 66, 1961, pp. 193.

[33] Lane, M. H., "The Development of an Artificial Satellite Theory Using Power-Law Atmospheric Density Representation," *AIAA Paper 65-35, 2nd Aerospace Sciences Meeting, New York, NY*, January 25-27, 1965.

[34] Lane, M. H. and Cranford, K. H., "An Improved Analytical Drag Theory for the Artificial Satellite Problem," *AIAA Paper 69-925, AIAA/AAS Astrodynamics Conference, Princeton, NJ*, August 20-22, 1969.

[35] Wiesel, W. E., *Modern Astrodynamics*, Aphelion Press, 2nd ed., 2010.

[36] Coffey, S. L., Neal, H. L., Visel, C. L., and Conolly, P., "Demonstration of a Special-Perturbations-Based Catalog in the Naval Space Command System," *AAS Paper 98-113, AAS/AIAA Space Flight Mechanics Meeting, 9-11 February 1998, Monterey, California*.

[37] Vinti, J. P., "Theory of an Accurate Intermediary Orbit for Satellite Astronomy," *Journal of Research of the National Bureau of Standards*, Vol. 65B, 1961, pp. 169–201.

[38] Vinti, J. P., "Formulae for an Accurate Intermediary Orbit of an Artificial Satellite," *The Astronomical Journal*, Vol. 66, 1961, pp. 514–516.

[39] Vinti, J. P., "Intermediary Equatorial Orbits of an Artificial Satellite," *Journal of Research of the National Bureau of Standards*, Vol. 66B, 1961, pp. 5–13.

[40] Vinti, J. P., "Zonal Harmonic Perturbations of an Accurate Reference Orbit of an Artificial Satellite," *Journal of Research of the National Bureau of Standards*, Vol. 67B, 1963, pp. 191–222.

[41] Vinti, J. P., "Inclusion of the Third Zonal Harmonic in an Accurate Reference Orbit of an Artificial Satellite," *Journal of Research of the National Bureau of Standards*, Vol. 70B, 1966, pp. 17–46.

[42] Vinti, J. P., "Improvement of the Spheroidal Method for Artificial Satellites," *The Astronomical Journal*, Vol. 74, 1969, pp. 25–34.

[43] Vinti, J. P., "Gaussian Variational Equations for Osculating Elements of an Arbitrary Separable Reference Orbit," *Celestial Mechanics*, Vol. 7, 1973, pp. 367–375.

[44] Barrar, R. B., "Some Remarks on the Motion of a Satellite of an Oblate Planet," *The Astronomical Journal*, Vol. 66, 1961, pp. 11–14.

[45] Morrison, F., *The Art of Modeling Dynamic Systems: Forecasting for Chaos, Randomness and Determinism*, Courier Corporation, 2012.

[46] Izsak, I. G., "A Theory of Satellite Motion About an Oblate Planet - A Second-Order Solution of Vinti's Dynamical Problem," *Smithsonian Astrophysical, Special Report No. 52*, 1960, pp. 1–54.

[47] Allen, W. A. and Knolle, W. E., "Differential Corrections Applied to the Izsak Equations of Artificial Satellite Motion," *The Astronomical Journal*, Vol. 69, 1964, pp. 393–401.

[48] Walden, H. and Watson, S., "Differential Corrections Applied to Vinti's Accurate Reference Satellite Orbit with Inclusion of the Third Zonal Harmonic," *NASA Technical Note D-4088*, 1967.

[49] Bonavito, N. L., "Computational Procedure for Vinti's Theory of an Accurate Intermediary Orbit," *NASA Technical Note D-1177*, October-December 1963.

[50] Bonavito, N. L., "Computational Procedure for Vinti's Accurate Reference Orbit with Inclusion of the Third Zonal Harmonic," *NASA Technical Note D-3562*, August 1966.

[51] Bonavito, N. L., Watson, S., and Walden, H., "An Accuracy and Speed Comparison of the Vinti and Brouwer Orbit Prediction Methods," *NASA Technical Note D-5203*, 1969.

[52] Gordon, R. A., Mistretta, G. D., and Watson, J., "A Comparison of Classical Analytical Theories for the Motion of Artificial Satellites," *Journal of Guidance and Control*, Vol. 2, 1978, pp. 184–189.

[53] Der, G. J. and Danchick, R., "Analytic and Numerical Error Covariance Matrix Propagation (for Spacecraft in Earth Orbital Environments)," *AAS 96-3661, AIAA/AAS Astrodynamics Conference, San Diego, CA, 29-31 July 1996*.

[54] Der, G. J., "An Elegant State Transition Matrix," *AAS 96-3660, AIAA/AAS Astrodynamics Conference, San Diego, CA, 29-31 July 1996*.

[55] Der, G. J., "About DerAstrodynamics," Accessed 19 May 2015, http://derastrodynamics.com/index.php?main_page=page&id=2.

[56] Meirovitch, L., *Methods of Analytical Dynamics*, Dover Publications, Inc, 2003.

[57] Duffy, L. M., *Orbital Resonances in the Vinti Solution*, Master's thesis, Air Force Institute of Technology, 2016.

[58] Kolmogorov, A. N., "On the Conservation of Conditionally Periodic Motion Under Small Perturbation of the Hamiltonian," *Dokl. Akad. Nauk. SSR.*, Vol. 98, January 1954, pp. 2–3.

[59] Arnold, V., "Proof of Kolmogorov's Theorem on the Preservation of Quasi-Periodic Motion Under Small Perturbations of the Hamiltonian," *Russian Mathematical Surveys*, Vol. 18, No. 5, 1963, pp. 9–36.

[60] Moser, J. K., "On Invariant Curves of Area Preserving Mappings of an Annulus," *Nachr. der Akad. Wiss. Gottingen, Math. Phys., Kl.*, Vol. IIa, Jan 1962, pp. 1–20.

[61] Wiesel, W. E., "Earth Satellite Perturbation Theories as Approximate KAM Tori," *Journal of the Astronautical Sciences*, Vol. 58, 2011, pp. 153–165.

[62] Celletti, A. and Chierchia, L., "KAM Stability for a Three-body Problem of the Solar System," *Z. angew. Math. Phys.*, Vol. 57, 2006, pp. 33–41.

[63] Wiesel, W. E., "Earth Satellite Orbits as KAM Tori," *Journal of Astronautical Sciences*, Vol. 56, 2008, pp. 151–162.

[64] Little, B. D., *Application of KAM Theorem to Earth Orbiting Satellites*, Master's thesis, Air Force Institute of Technology, 2009.

[65] Bisher, C. L., *Verification of KAM Theory on Earth Orbiting Satellites*, Master's thesis, Air Force Institute of Technology, 2010.

[66] Bordner, R. E., *Orbital Tori Construction Using Trajectory Following Spectral Methods*, Ph.D. thesis, Air Force Institute of Technology, 2009.

[67] Bordner, R. E. and Wiesel, W. E., "Spectral Decomposition of Orbital Tori," *Journal of Guidance, Control, and Dynamics*, Vol. 34, No. 2, 2011, pp. 504–512.

[68] Craft, C. T., *Formation Flight of Earth Satellites on KAM Tori*, Master's thesis, Air Force Institute of Technology, 2009.

[69] Yates, M. W., *Stochastic Orbit Prediction Using KAM Theory*, Master's thesis, Air Force Institute of Technology, 2011.

[70] Hagen, L. J., *Effects of Air Drag and Lunar Third-body Perturbations on Orbital Motion Near a Reference KAM Torus*, Master's thesis, Air Force Institute of Technology, 2011.

[71] Dunk, A. B., *Applying KAM Theory to Highly Eccentric Orbits*, Master's thesis, Air Force Institute of Technology, 2014.

[72] Frey, G. R., *KAM Torus Frequency Generation from Two-line Element Sets*, Master's thesis, Air Force Institute of Technology, 2011.

[73] Wiesel, W. E., "A Theory of Low Eccentricity Earth Satellite Motion," *Journal of Asttronautical Sciences*, Vol. 59, 2012, pp. 629–649.

[74] Abay, R., *KAM Torus Orbit Prediction From Two Line Element Sets*, Master's thesis, Air Force Institute of Technology, 2014.

[75] Wiesel, W. E., *Modern Orbit Determination*, Aphelion Press, 2nd ed., 2010.

[76] Vallado, D. A., "SGP4 Orbit Determination," *AIAA/AAS Astrodynamics Specialist Conference and Exhibit, Honolulu, Hawaii*, 2008.

[77] Abramowitz, M. and Segun, I., *Handbook of Mathematical Functions*, Dover, 1965, Ch 25, p. 883.

[78] Regan, F. J. and Anandakrishnan, S. M., *Dynamics of Atmospheric Re-Entry*, AIAA Education Series, 1993.

[79] Lynn, W. J., "A Military Strategy for the New Space Environment," *The Washington Quarterly*, Vol. 34, Summer 2011, pp. 7–16.

REPORT DOCUMENTATION PAGE

Form Approved
OMB No. 0704–0188

1. REPORT DATE *(DD–MM–YYYY)*	2. REPORT TYPE	3. DATES COVERED *(From — To)*
15–09–2016	Dissertation	October 2012 - September 2016

4. TITLE AND SUBTITLE

Orbit Determination Using Vinti's Solution

5a. CONTRACT NUMBER

5b. GRANT NUMBER

5c. PROGRAM ELEMENT NUMBER

6. AUTHOR(S)

Wright, Steven P., Major, USAF

5d. PROJECT NUMBER

5e. TASK NUMBER

5f. WORK UNIT NUMBER

7. PERFORMING ORGANIZATION NAME(S) AND ADDRESS(ES)

Air Force Institute of Technology
Graduate School of Engineering and Management (AFIT/EN)
2950 Hobson Way
Wright-Patterson AFB, OH 45433-7765

8. PERFORMING ORGANIZATION REPORT NUMBER

AFIT-ENY-DS-16-S-067

9. SPONSORING / MONITORING AGENCY NAME(S) AND ADDRESS(ES)

10. SPONSOR/MONITOR'S ACRONYM(S)

11. SPONSOR/MONITOR'S REPORT NUMBER(S)

12. DISTRIBUTION / AVAILABILITY STATEMENT

Distribution Statement A
Approved for Public Release; Distribution Unlimited

13. SUPPLEMENTARY NOTES

14. ABSTRACT

Orbital altitudes congested with spacecraft and debris combined with recent collisions have all but negated the Big Sky Theory. As the sheer number of orbital objects to track grows unbounded so does interest in prediction methods that are rapid and minimally computational. Claimed as the "other solvable solution," the recently completed solution to orbital motion about the earth, based on Vinti's method and including the major effects of the equatorial bulge, opens up the prospect of much more accurate analytical models for space situational awareness. A preliminary examination of this solution is presented. A numerical state transition matrix is found using Lagrange partial derivatives to implement a nonlinear least squares fitting routine. Orbit fits using only the solvable solution for non-circular, non-equatorial trajectories less than 60 degrees inclination are on the order of a few hundred meters with projected, average error growth of less than a kilometer per day which is similar to the expected performance of the Air Force's method. Also, a classical perturbations approach to incorporate the dissipative effects of air drag using Hamiltonian action and angle formulation is developed. Predicted drag effects are 97.5% correct after one day and 87% correct after five days when compared to an integrated truth. Results are validated by performing a similar method on the two body problem.

15. SUBJECT TERMS

Vinti's Solution, Orbit Determination, Action-angles, Air Drag

16. SECURITY CLASSIFICATION OF:			17. LIMITATION OF ABSTRACT	18. NUMBER OF PAGES	19a. NAME OF RESPONSIBLE PERSON
a. REPORT	b. ABSTRACT	c. THIS PAGE			Dr. William E. Wiesel (ENY)
U	U	U	UU	116	19b. TELEPHONE NUMBER *(include area code)* (937) 255-6565 x4312 william.wiesel@afit.edu